

NAVAL POSTGRADUATE SCHOOL MONTEREY, CALIFORNIA



THESIS

NUMERICAL ANALYSIS OF OSCILLATING FLOW ABOUT A CIRCULAR CYLINDER

by

Craig D. Hanson

December, 1995

Thesis Advisor:

T. Sarpkaya

Approved for public release; distribution is unlimited.

19960327 071

DTIC QUALITY INSPECTED 1

REPORT DOCUMENTATION PAGE			Form Approved OMB No. 0704-0188	
Public reporting burden for this collection of information is estimated to average 1 hour per response, including the time for reviewing instruction, searching existing data sources, gathering and maintaining the data needed, and completing and reviewing the collection of information. Send comments regarding this burden estimate or any other aspect of this collection of information, including suggestions for reducing this burden, to Washington Headquarters Services, Directorate for Information Operations and Reports, 1215 Jefferson Davis Highway, Suite 1204, Arlington, VA 22202-4302, and to the Office of Management and Budget, Paperwork Reduction Project (0704-0188) Washington DC 20503.				
1. AGENCY USE ONLY (Leave blank)		2. REPORT DATE December, 1995		3. REPORT TYPE AND DATES COVERED Master's Thesis
4. TITLE AND SUBTITLE Numerical Analysis of Oscillating Flow About a Circular Cylinder			5. FUNDING NUMBERS	
6. AUTHOR(S) Craig D. Hanson				
7. PERFORMING ORGANIZATION NAME(S) AND ADDRESS(ES) Naval Postgraduate School Monterey CA 93943-5000			8. PERFORMING ORGANIZATION REPORT NUMBER	
9. SPONSORING/MONITORING AGENCY NAME(S) AND ADDRESS(ES)			10. SPONSORING/MONITORING AGENCY REPORT NUMBER	
11. SUPPLEMENTARY NOTES The views expressed in this thesis are those of the author and do not reflect the official policy or position of the Department of Defense or the U.S. Government.				
12a. DISTRIBUTION/AVAILABILITY STATEMENT Approved for public release; distribution is unlimited.			12b. DISTRIBUTION CODE	
13. ABSTRACT (maximum 200 words) The numerical experiments, carried out through the use of a pressure-velocity coupled method to solve the Favre Averaged Navier-Stokes equations, on steady and sinusoidally oscillating flows at five different Keluegan-Carpenter numbers, and three periodicity levels are described. A second-order in time, second-order in space, second-level predictor-corrector finite difference scheme has been used. The solutions were solved by the CFD-ACE program from the CFD Research Corporation. The analysis has produced in-line force coefficients comparable to those obtained experimentally for sinusoidally-oscillating flows.				
14. SUBJECT TERMS Numerical Calculations, Cylinder, Oscillating Flow, Co-existing flow, Harmonically oscillating flow			15. NUMBER OF PAGES 78	
			16. PRICE CODE	
17. SECURITY CLASSIFICATION OF REPORT Unclassified	18. SECURITY CLASSIFICATION OF THIS PAGE Unclassified	19. SECURITY CLASSIFICATION OF ABSTRACT Unclassified	20. LIMITATION OF ABSTRACT UL	

NSN 7540-01-280-5500

Standard Form 298 (Rev. 2-89)
Prescribed by ANSI Std. Z39-18 298-102

Approved for public release; distribution is unlimited.

**NUMERICAL ANALYSIS OF
OSCILLATING FLOW ABOUT A CIRCULAR CYLINDER**

Craig D. Hanson
Lieutenant Commander, United States Navy
B.S., Iowa State University, 1982
M.S., Naval Postgraduate School, 1988


Submitted in partial fulfillment
of the requirements for the degree of

MASTER OF SCIENCE IN MECHANICAL ENGINEERING

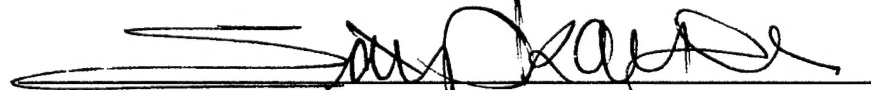
from the


**NAVAL POSTGRADUATE SCHOOL
December 1995**

Author:


Craig D. Hanson

Approved by:


T. Sarpkaya, Thesis Advisor


Matthew D. Kelleher, Chairman
Department of Mechanical Engineering

ABSTRACT

The numerical experiments, carried out through the use of a pressure-velocity coupled method to solve the Favre Averaged Navier-Stokes equations, on steady and sinusoidally oscillating flows at five different Keluegan-Carpenter numbers, and three periodicity levels are described. A second-order in time, second-order in space, second-level predictor-corrector finite difference scheme has been used. The solutions were solved by the CFD-ACE program from the CFD Research Corporation. The analysis has produced in-line force coefficients comparable to those obtained experimentally for sinusoidally-oscillating flows.

TABLE OF CONTENTS

I. INTRODUCTION	1
II. BACKGROUND STUDIES	3
III. NUMERICAL REPRESENTATION	7
A. COMPUTATIONAL METHOD	7
B. CALCULATION OF FORCE COEFFICIENTS	10
C. GRID DEFINITION	11
D. BOUNDARY CONDITIONS	12
E. FLOW GENERATION	12
F. PARAMETER OPTIONS	13
IV. DISCUSSION OF RESULTS	15
A. INTRODUCTION	15
B. LOW FLOW VERIFICATION	15
C. HIGH FLOW VERIFICATION	16
D. OSCILLATING FLOWS	17
V. CONCLUSIONS	21
APPENDIX: FIGURES	23
REFERENCES	57
INITIAL DISTRIBUTION LIST	59

LIST OF FIGURES

Figure 1. Grid in the Physical Domain	23
Figure 2. Flow About a Square Cylinder at $Re = 400$	23
Figure 3. Flow About a Circular Cylinder at $Re = 400$	24
Figure 4. Flow About a Circular Cylinder at $Re = 400$	24
Figure 5. In-Line Force Coefficient vs t/T , $\beta = 1000$, $K = 8$, $Re = 8,000$	25
Figure 6. Transverse Force Coefficient vs t/T , $\beta = 1000$, $K = 8$, $Re = 8,000$	25
Figure 7. In-Line Force Coefficient vs t/T , $\beta = 1000$, $K = 12$, $Re = 12,000$	26
Figure 8. Transverse Force Coefficient vs t/T , $\beta = 1000$, $K = 12$, $Re = 12,000$	26
Figure 9. In-Line Force Coefficient vs t/T , $\beta = 1000$, $K = 20$, $Re = 20,000$	27
Figure 10. Transverse Force Coefficient vs t/T , $\beta = 1000$, $K = 20$, $Re = 20,000$	27
Figure 11. In-Line Force Coefficient vs t/T , $\beta = 1000$, $K = 25$, $Re = 25,000$	28
Figure 12. Transverse Force Coefficient vs t/T , $\beta = 1000$, $K = 25$, $Re = 25,000$	28
Figure 13. In-Line Force Coefficient vs t/T , $\beta = 1000$, $K = 35$, $Re = 35,000$	29
Figure 14. Transverse Force Coefficient vs t/T , $\beta = 1000$, $K = 35$, $Re = 35,000$	29
Figure 15. In-Line Force Coefficient vs t/T , $\beta = 2000$, $K = 8$, $Re = 16,000$	30
Figure 16. Transverse Force Coefficient vs t/T , $\beta = 2000$, $K = 8$, $Re = 16,000$	30
Figure 17. In-Line Force Coefficient vs t/T , $\beta = 2000$, $K = 12$, $Re = 24,000$	31
Figure 18. Transverse Force Coefficient vs t/T , $\beta = 2000$, $K = 12$, $Re = 24,000$	31
Figure 19. In-Line Force Coefficient vs t/T , $\beta = 2000$, $K = 20$, $Re = 40,000$	32
Figure 20. Transverse Force Coefficient vs t/T , $\beta = 2000$, $K = 20$, $Re = 40,000$	32
Figure 21. In-Line Force Coefficient vs t/T , $\beta = 2000$, $K = 25$, $Re = 50,000$	33
Figure 22. Transverse Force Coefficient vs t/T , $\beta = 2000$, $K = 25$, $Re = 50,000$	33
Figure 23. In-Line Force Coefficient vs t/T , $\beta = 2000$, $K = 35$, $Re = 70,000$	34
Figure 24. Transverse Force Coefficient vs t/T , $\beta = 2000$, $K = 35$, $Re = 70,000$	34
Figure 25. In-Line Force Coefficient vs t/T , $\beta = 3100$, $K = 8$, $Re = 24,800$	35
Figure 26. Transverse Force Coefficient vs t/T , $\beta = 3100$, $K = 8$, $Re = 24,800$	35

Figure 27. In-Line Force Coefficient vs t/T , $\beta = 3100$, $K = 12$, $Re = 37,200$	36
Figure 28. Transverse Force Coefficient vs t/T , $\beta = 3100$, $K = 12$, $Re = 37,200$	36
Figure 29. In-Line Force Coefficient vs t/T , $\beta = 3100$, $K = 20$, $Re = 62,000$	37
Figure 30. Transverse Force Coefficient vs t/T , $\beta = 3100$, $K = 20$, $Re = 62,000$	37
Figure 31. In-Line Force Coefficient vs t/T , $\beta = 3100$, $K = 25$, $Re = 77,500$	38
Figure 32. Transverse Force Coefficient vs t/T , $\beta = 3100$, $K = 25$, $Re = 77,500$	38
Figure 33. In-Line Force Coefficient vs t/T , $\beta = 3100$, $K = 35$, $Re = 108,500$	39
Figure 34. Transverse Force Coefficient vs t/T , $\beta = 3100$, $K = 8$, $Re = 108,500$	39
Figure 35. Vorticity Plot for an Oscillatory Flow About a Circular Cylinder at $\beta = 1000$, $K = 8$, $Re = 8,000$ (Steps 1 - 6 in Increments of 45 Degrees)	40
Figure 36. Vorticity Plot for an Oscillatory Flow About a Circular Cylinder at $\beta = 1000$, $K = 8$, $Re = 8,000$ (Steps 7 - 12 in Increments of 45 Degrees)	41
Figure 37. Vorticity Plot for an Oscillatory Flow About a Circular Cylinder at $\beta = 1000$, $K = 12$, $Re = 24,000$ (Steps 1 - 6 in Increments of 22.5 Degrees)	42
Figure 38. Vorticity Plot for an Oscillatory Flow About a Circular Cylinder at $\beta = 1000$, $K = 12$, $Re = 24,000$ (Steps 7 - 12 in Increments of 22.5 Degrees)	43
Figure 39. Vorticity Plot for an Oscillatory Flow About a Circular Cylinder at $\beta = 1000$, $K = 12$, $Re = 24,000$ (Steps 12 - 18 in Increments of 22.5 Degrees)	44
Figure 40. Vorticity Plot for an Oscillatory Flow About a Circular Cylinder at $\beta = 1000$, $K = 12$, $Re = 24,000$ (Steps 18 - 24 in Increments of 22.5 Degrees)	45
Figure 41. Vorticity Plot for an Oscillatory Flow About a Circular Cylinder at $\beta = 1000$, $K = 20$, $Re = 20,000$ (Steps 1 - 6 in Increments of 45 Degrees)	46
Figure 42. Vorticity Plot for an Oscillatory Flow About a Circular Cylinder at $\beta = 1000$, $K = 20$, $Re = 20,000$ (Steps 7 - 12 in Increments of 45 Degrees)	47
Figure 43. Streamline Plot for an Oscillatory Flow About a Circular Cylinder at $\beta = 1000$, $K = 20$, $Re = 20,000$ (Steps 1 - 6 in Increments of 45 Degrees)	48
Figure 44. Streamline Plot for an Oscillatory Flow About a Circular Cylinder at $\beta = 1000$, $K = 20$, $Re = 20,000$ (Steps 7 - 12 in Increments of 45 Degrees)	49

Figure 45. Vorticity Plot for an Oscillatory Flow About a Circular Cylinder at $\beta = 2000$, K = 20, Re = 40,000 (Steps 1 - 6 in Increments of 45 Degrees)	50
Figure 46. Vorticity Plot for an Oscillatory Flow About a Circular Cylinder at $\beta = 2000$, K = 20, Re = 40,000 (Steps 7 - 12 in Increments of 45 Degrees)	51
Figure 47. Vorticity Plot for an Oscillatory Flow About a Circular Cylinder at $\beta = 3100$, K = 35, Re = 108,500 (Steps 1 - 6 in Increments of 45 Degrees)	52
Figure 48. Vorticity Plot for an Oscillatory Flow About a Circular Cylinder at $\beta = 3100$, K = 35, Re = 108,500 (Steps 1 - 6 in Increments of 45 Degrees)	53
Figure 49. Streamline Plot for an Oscillatory Flow About a Circular Cylinder at $\beta = 3100$, K = 35, Re = 108,500 (Steps 1 - 6 in Increments of 45 Degrees)	54
Figure 50. Streamline Plot for an Oscillatory Flow About a Circular Cylinder at $\beta = 3100$, K = 35, Re = 108,500 (Steps 7 - 12 in Increments of 45 Degrees)	55

LIST OF TABLES

Table 1.	Comparison of Experimental and Historical In-Line Force Coefficients and Strouhal Numbers at Low Reynolds Numbers	16
Table 2.	Sensitivity of Parameters on the In-Line Force Coefficient	18
Table 3.	Oscillating Flow In-Line Force Coefficient Results	19

NOMENCLATURE

C_{IL}	= in-line force coefficient
C_L	= transverse force coefficient
D	= diameter
K	= Keulegan-Carpenter Number = $U_M T/D$
p_s	= pressure on cylinder
R	= cylinder radius
Re	= Reynolds number = $U_M D/\nu$
r	= radial distance
T	= period of oscillations
t	= time
U	= time dependent velocity
U_M	= maximum velocity in pure sinusoidal flow
β	= $D^2/\nu T$
μ	= dynamic viscosity
ν	= kinematic viscosity
ρ	= density
θ	= angular position
ψ	= stream function
ω	= vorticity

ACKNOWLEDGMENTS

For the support and guidance of Naval Engineering facility members of the Naval Postgraduate School whose instructions and wisdom over the last two years has led to the completion of course work for this degree, I express my sincere appreciation.

The funding, which made possible the accessibility for the computer and program code, was made possible by the Office of Naval Research. Their continued support for research of world class professors has made this a life broadening educational experience.

Many others have given me help along the way. Mr. Dave Marco has given me tremendous support using the ME computer lab, setup of the SGI computer, and software loading. Mr. Lyle Johnson, Mr. Milind Talpallikar, and Mr. Gary Hufford of the CFD Research Corporation provided their insights and introduction to the CFD-ACE program and code. LCDR Marc De Angelis was instrumental in my introduction to the code. Dr. Walter P. Wolfe of Sandia National Laboratories supplied the specific change to program for the use on bluff bodies.

Finally, my loving appreciation goes to my wife Carole and daughter Jennifer for their continual support and understanding.

I. INTRODUCTION

The study of time-dependent flows past bluff bodies has historically been the focus of a great deal of scientific attention owing to its relevance to many and diverse applications, ranging from submerged structures to hot wire anemometers. Some forty years ago, Keulegan and Carpenter commenced the methodical investigation of the fluid-structure interactions which occur when bodies are immersed in unsteadily flowing fluids. Today, the effect of the pertinent parameters, such as Reynolds number, Keulegan-Carpenter number and relative roughness, to name a few, is much better understood thanks to ongoing research in this area. In spite of this progress, real time prediction of the forces caused by unsteady flows on submerged objects, such as those acting on an underwater robotic arm or an offshore oil rig, seriously challenges our current theoretical and computational capabilities.

One of the principal empirical tools used by the engineer to solve the problems described above, Morison's equation, is only reliable in predicting forces and moments in highly idealized conditions with very low or very high flow oscillation periods. Additionally, most real-life problems involve flows in the turbulent regime, further increasing the level of difficulty of both analytical and numerical solutions.

Given the cost and complexity of the laboratory apparatuses required to reproduce real life flow conditions, theoretical and experimental advances have been paralleled by a considerable research effort in the area of computational fluid dynamics to assist in the solution of problems related to bodies immersed in unsteadily flowing fluids. Progress in numerical techniques and the ever increasing power of present day computers are finally making it possible to overcome the barrier historically imposed by the physical and numerical instabilities which have caused the modeling of turbulent flows particularly challenging in the past.

Whereas, until recently, numerical experimentation has only been successful in determining flow patterns, Strouhal numbers and force coefficients for flow regimes within selected ranges of relatively low Reynolds numbers, it is now possible to obtain useful data

for more turbulent flows exhibiting extensive separation. Furthermore, commercial software is becoming available which affords researchers much greater flexibility than the ad hoc codes previously generated to solve very specific categories of problems, allowing for the analysis of a much broader gamut of flow conditions.

Unfortunately, in spite of such great flexibility, modern software does not yet absolve the user from having to fine-tune the code by the judicious selection of parameters, numerical techniques and turbulence models. Moreover, even after the available numerical schemes have undergone a considerable amount of refinement, experimentally obtained results cannot be exactly duplicated in all cases.

If complete and accurate solutions are not yet always achievable, however, approximate solutions can certainly aid in expanding our current level of understanding and provide the engineer with a valuable tool to improve design optimization. From the above discussion, it can be inferred that a benchmark body of reliable calculations, performed using the most sophisticated and carefully selected set of computational tools, is required to calibrate our current empirical equations and experimental results.

The objective of this investigation is to lay the foundations for such an endeavor and improve our current ability to predict the effects of time-dependent turbulent flows over circular cylinders through the use of a state of the art commercial code generated by CFD Research Corporation (CFDRC). Whenever possible, the results achieved have been compared to those obtained experimentally. Besides their intrinsic value, these results will aid in pointing out some of the strengths and weaknesses of the code and hopefully add to our understanding of the physics of flow types not previously analyzed.

II. BACKGROUND STUDIES

Research at the Naval Postgraduate School (Sarpkaya 1976) resulted in a comprehensive series of experiments concerning sinusoidally oscillating flow about smooth and rough bodies, and introduced the parameter $\beta (= Re/K)$ to assess the influence of scale in periodic flows. The findings demonstrated a dependence of the force-transfer coefficients on Re , K , and k/D . The work continued involving a coexisting flow as specified by $U = U_o + U_m \sin (2\pi t/T)$ in which U_o is the steady mean velocity and U_m is the amplitude of sinusoidal oscillations (Storm 1980).

Numerous numerical predictions of the Strouhal number, the pressure distribution, and the evolution of the lift and drag forces in impulsively-started steady ambient flows have been performed to replicate this effort. No computational attempt was made to investigate the effect of the initial acceleration, prior to the establishment of a steady uniform flow, on the characteristics of the resulting time-dependent flow (Putzig 1991). Here, only the more recent investigations will be reviewed.

A finite-difference analysis of the Navier-Stokes equations for a sinusoidally oscillating ambient flow about a circular cylinder at $K = 5$ ($Re = 1000$) and $K = 7$ ($Re = 700$) has been attempted (Baba Miyata 1987), assuming a physically unrealistic symmetric wake in both simulations. Their results have shown that the calculations can be carried out only for short times (less than two cycles of flow oscillation) with a non-super computer.

A similar method was used to analyze three cases ($K = 5, 7$, and 10) at higher Reynolds numbers around 10^4 (Murashige 1989). The flow was perturbed by artificial means to trigger asymmetry. At $K = 10$, a transverse vortex street appeared, in agreement with experimental observations. A Simulation using multi-discrete vortices (with wore), simulated the sinusoidally oscillating flow about a circular cylinder and the decelerating flow about camber plates (Mostafa 1987). His calculations for $K = 12$ reproduced correctly for the first time the transverse vortex street observed experimentally. However, the calculated forces were somewhat larger than those measured (Putzig 1991).

A series of numerical experiments with sinusoidally oscillating as well as co-existing laminar flows at relatively small K values yielded total force coefficients which were not only highly stable, but also in reasonable agreement with those obtained experimentally. The numerical experiments with co-existing flows produced extremely interesting flow features. For relative current velocities V_r (U_o/U_m) = 0.7 - 0.8, the vortices shed nearly symmetrically at each cycle. However, they formed a three-row vortex street only in the range of $V_r = 0.6$ -0.7. For V_r larger than about one, the vortex wake returned to the asymmetric mode, as in a regular vortex street. The calculations of resistance in co-existing flows showed that the inertia as well as the drag coefficients for $K = 4 - 6$ were in reasonable agreement with experimental data (Sarpkaya, Putzig, Gordon, Wang, & Dalton 1992).

Work has also centered on the square cylinder. Early work was flawed by the use of central differencing at large cell Reynolds numbers. This led to spatial oscillations ahead of the rectangle. Improvements were made by using a time differencing and third-order upwinding on the convective terms, although, because of standard centered-diffusion differencing, it was overall second-order accurate spatially for non-zero kinematic viscosity. This was tried for a Reynolds number under 3,000 (Davis & Moore 1982). The use of the modified K -epsilon (k - ϵ) and K -omega (k - Ω) models on a square cylinder led to agreement comparable with that obtained formerly only with the second-moment closure, and with respect to the turbulence energy led to markedly superior behavior in the near-field region (Kato & Launder 1993).

Aerodynamic research on airfoils further showed the capabilities of the k - ϵ model. The model did require more grid points than previous models like the Baldwin-Barth model but was significantly better at computing maximum lift conditions and flap boundary-layer separation (Rogers 1994).

Most of the initial numerical codes were university or government (NASA) generated but now the commercial sector has started to produce software for fluid flows and data visualization. The CFD Research Corporation (CFDRC) created a general-purpose Computational Fluid Dynamics (CFD) code with multi-domain solution capability. The

initial results showed the program to be able to predict Strouhal numbers in uniform flow at higher Reynolds numbers and forces but questioned the ability to capture the high turbulence intensity levels present in the near-wake region (Singhal & Avva 1994). The program was further tested in uniform flow using the $k-\epsilon$ and RNG (Re-Normalization Group) model at Reynolds numbers over 10^6 . It was able to reasonably reproduce Strouhal numbers but was not tested for force coefficients (Habchi & Hufford 1995).

III. NUMERICAL REPRESENTATION

A. COMPUTATIONAL METHOD

Here only a brief description of the computational method is presented. A more in depth description is given by CFD-ACE Theory Manual.

The fluid is assumed to be two-dimensional, incompressible and viscous. The governing equations of the code are the Favre (density) Averaged Navier-Stokes (FANS) equations which are solved by a pressure-velocity coupled method.

The Navier-Stokes equations are averaged over time or ensemble of statistically equivalent flows to yield averaged equations. In the averaging process, a flow quantity u_i is decomposed into mean and fluctuating parts. The Favre averages use

$$u = \tilde{u} + u_i'' \text{ where } \tilde{u} = \overline{\rho\phi}/\bar{\rho} \quad (1)$$

The overbar denotes Reynolds averaging while tilde denotes Favre averaging. The time period of averaging, T , should be large compared to the fluctuation time scale so that mean quantities are stationary over a number of samples.

The Favre averaged continuity equation is

$$\frac{\partial \bar{\rho}}{\partial t} + \frac{\partial}{\partial x_j} (\bar{\rho} \tilde{u}_j) = 0 \quad (2)$$

Similarly when the Navier-Stokes (NS) equations are averaged, the following FANS equation is obtained (Cebeci & Smith 1974):

$$\frac{\partial}{\partial t} (\bar{\rho} \tilde{u}_j) + \frac{\partial}{\partial x_j} (\bar{\rho} \tilde{u}_i \tilde{u}_j) = - \frac{\partial \bar{p}}{\partial x_i} + \frac{\partial}{\partial x_j} [\bar{\mu} (\frac{\partial \tilde{u}_i}{\partial x_j} + \frac{\partial \tilde{u}_j}{\partial x_i} - \frac{\partial \tilde{u}_m}{\partial x_m} \delta_{ij})] + \frac{\partial}{\partial x_j} (-\bar{\rho} \overline{u_i' u_j'}) \quad (3)$$

The FANS equation contains less information than the full NS equations, but have additional unknown terms - called the Reynolds stresses, $(-\bar{\rho} \overline{u_i' u_j'})$. The correlations between the

fluctuation components arise in the averaging process and require modeling for closure of the FANS equation. The program treats the Reynolds stress as a linear function of the mean strain and is incorporated in all the turbulence models of the code.

Each flow variable is governed by a partial differential equation (PDE) which is numerically solved to obtain a discrete solution for that variable. No governing PDE for pressure is present. Pressure-based methods utilize the continuity equation to formulate an equation for pressure. The code uses a variant of the Semi-Implicit Method for Pressure Linked Equations (SIMPLE) (Comini & Del Giudice 1987) which iteratively creates an equation for pressure-correction from the continuity equation. The key in the calculation of the velocity field is the unknown pressure gradients. The pressure gradients can be written as sums of estimated (*) and correction (') values:

$$\frac{\partial p}{\partial y} = \left(\frac{\partial p}{\partial y}\right)^* + \left(\frac{\partial p}{\partial y}\right)' = \left(\frac{\partial p}{\partial y}\right)^n + \left(\frac{\partial p}{\partial y}\right)' \quad (4)$$

where the pressure gradients at the previous step n make an estimate. The conservation of momentum can be linearized and split for a constant property and two-dimensional flow to yield for the v case:

$$\left(\frac{\partial v}{\partial t}\right)^* + \left(\frac{\partial v}{\partial t}\right)' \approx \frac{1}{Re} \left[\frac{\partial}{\partial y} \left(\mu_e \frac{\partial v^*}{\partial y} \right) + \frac{\partial}{\partial z} \left(\mu_e \frac{\partial v^*}{\partial z} \right) \right] - (v^n \frac{\partial v^*}{\partial y} + w^n \frac{\partial v^*}{\partial z}) + V_y^n - \left(\frac{\partial p}{\partial y}\right)^n - \frac{\partial p'}{\partial y} \quad (5)$$

Solving for the components of accelerations marked with asterisks via an implicit scheme in the time integration:

$$\left(\frac{\partial v}{\partial t}\right)^* = \frac{1}{Re} \left[\frac{\partial}{\partial y} \left(\mu_e \frac{\partial v^*}{\partial y} \right) + \frac{\partial}{\partial z} \left(\mu_e \frac{\partial v^*}{\partial z} \right) \right] - (v^n \frac{\partial v^*}{\partial y} + w^n \frac{\partial v^*}{\partial z}) + V_y^n - \left(\frac{\partial p}{\partial y}\right)^n \quad (6)$$

and

$$\left(\frac{\partial v}{\partial t}\right)' = \frac{\partial p'}{\partial y} \quad (7)$$

After enforcing continuity and rearranging, the following is obtained:

$$\frac{\partial^2 p'}{\partial y^2} + \frac{\partial^2 p'}{\partial z^2} = \frac{1}{\Delta t} \left(\frac{\partial v^*}{\partial y} + \frac{\partial w^*}{\partial z} \right) \quad (8)$$

Equation (8) is a Poisson-like equation for the pressure correction whose initial boundary conditions are:

$$p' = 0 \quad (9)$$

where the pressure is known and:

$$\frac{\partial p'}{\partial n} = 0 \quad (10)$$

elsewhere . Once the pressure correction has been determined, the corresponding velocity corrections v' can be computed from equations (7). The pressures and velocities can be updated:

$$p^{n+1} = p^n + p' \quad (11)$$

$$v^{n+1} = v^* - \frac{\partial p'}{\partial y} \Delta t = v^* + v' \quad (12)$$

The important operations, in the order of execution, are:

1. Estimate (guess) the pressure field;
2. Using the estimated pressure, solve the momentum equations to obtain approximate velocity v^* ;
3. By equation (8) calculate the pressure correction p' that enforces continuity;
4. Use the pressure correction p' to update the pressure and velocity fields;
5. Return to step 2) and repeat until convergence, or steady state, has been reached.

B. CALCULATION OF THE FORCE COEFFICIENTS

The in-line and transverse force coefficients are determined from the combined contributions of the shear and pressure forces acting on the cylinder. The viscous forces are calculated from $\tau_s = \mu \omega$. The total in-line force then reduces to

$$F_{IL} = - \int_0^{2\pi} (p_s \cdot \cos(\theta) R) d\theta - \int_0^{2\pi} \mu \omega \sin(\theta) d\theta \quad (13)$$

and the total lift force as

$$F_L = - \int_0^{2\pi} (p_s \cdot \sin(\theta) R) d\theta - \int_0^{2\pi} \mu \omega \cos(\theta) d\theta \quad (14)$$

The program performs this integration by calculating the shear and pressure forces on the wall for each Cartesian axis. The pressure in each cell block, which has a wall boundary, is subdivided into its coordinate components and then multiplied by its area normal to that direction. The pressure forces are then summed for all of the cell block wall boundaries. The shear force is calculated in each cell by:

$$F_x Shear = \mu \frac{u}{\delta} A_w \approx \tau_w A_w \quad (15)$$

where δ is the distance from the cell center to the cell wall, A_w is the cell wall length tangential to a given direction and the u is the coordinate velocity at the cell center. The total shear force in a given direction is then found by summing the cell forces.

The force coefficients are then formulated:

$$C_{IL} = \frac{\sum F_x Pressure + \sum F_x Shear}{0.5 \rho U^2 D} \quad (16)$$

and

$$C_L = \frac{\sum F_y Pressure + \sum F_y Shear}{0.5 \rho U^2 D} \quad (17)$$

C. GRID DEFINITION

The choice of grid definition is significant in capturing the gradients of both the vorticity and the stream function, particularly where they are large. The region near the cylinder wall is the most critical one since this is where the relative velocity gradients necessitates a higher density of cell mesh. This same density can be extended radially to the desired boundary size to maintain the accuracy of the vortices generated beyond the separation point. This, in turn requires a high number of cells which increases CPU time. To obtain a solution in a realistic time of 24 to 48 hours for just a couple of vortex shedding events, one must make a trade off between the desire to fully capture the fluid dynamics and the computational time. The most common way is to limit the grid density in less critical regions. The penalty is the loss in accuracy of vortex strengths as they move away from the wall. In steady flow, this is not as critical. A vortex influences the upstream flow but does not return to the cylinder. However, this is not true in oscillating flow and the judicial consideration of the wake-return problem is of utmost importance.

A square grid of uniform density can easily be generated for a uniform flow about a square cylinder. Such a grid will capture any event, at any point, but computationally it is not very efficient in the areas away from the cylinder where less grid density is desired. The symmetry of the geometry does reduce the grid generation and CPU time. The square is not the primary concern of this investigation and a purely square mesh does not work for circular cylinders.

A polar plot, with the circular cylinder in the center, with radially increasing cell size is the optimum solution, but the boundaries for flow limits the viability of this grid. A cross shape quadrant approach can still capture in most of the desired effects as shown in Figure 1. To achieve a higher density of mesh points near the cylinder surface, a power distribution may be utilized in the radial direction. The actual specifics of the grid is described in Chapter IV.

D. BOUNDARY CONDITIONS

Four boundary conditions are utilized in this investigation: symmetry, wall, prescribed pressure exit, and interface. At a symmetry boundary, the velocity normal to the boundary is set to zero and, for all variables, the gradient normal to the boundary is set to zero. The velocity normal to the boundary is also set to zero at wall boundaries. In both cases, this results in no mass source for the pressure correction equation. The boundary pressure correction value of zero is linked to the pressure correction equation in the prescribed pressure exit which results in mass flow into or out of the region. Interface is used for continuity between domains (regions) of the grid and has no property definition capabilities.

The program has two additional types of exit and inlet boundary conditions, but these are not used. The exit boundary conditions are an extrapolation intended for use in supersonic flow models. The inlet boundary conditions include prescribed mass flux and prescribed total pressure. Inlet boundaries, as defined by the program, allow only in flux of mass. Thus, to simulate boundaries that are subjected to by-directional flow, outlet prescribed pressure boundaries are utilized (CFDRC 1993).

E. FLOW GENERATION

The desired flow for the investigation is an oscillating flow specified by:

$$U = U_o + U_m \sin(2\pi t/T) \quad (18)$$

where U_o is the steady mean velocity, T is the period of the oscillation, t is time and, U_m is the amplitude of sinusoidal oscillations. The code allows entries of flow by velocity. However, oscillating flow could not be generated in this manner. An alternate manner of control by boundary pressure does generate the desired velocity. By placing equal magnitude positive and negative pressures on opposite sides of the boundaries, the required velocity can be formulated by:

$$Pressure = \frac{2\pi}{T} \rho U_m \Delta x \quad (19)$$

where Δx is the distance from the boundary wall to the center of the cylinder for a symmetric mesh.

D. PARAMETER OPTIONS

The CFD-ACE is a menu driven program that creates a formatted input file which can be externally edited. This section will discuss only those parameters that apply to exterior flow on bluff bodies and require additional emphasis beyond the CFD-Command Language Manual.

The program has two temporal options. The default is Euler and works with no difficulties. Crank-Nicholson is the non-default variable. The menu creates the option but fails to generate the correct spelling and requires exterior editing of the input file by changing the command to "CRANK_NICHOLSON".

Four spatial options are available for the user. The most robust is the default upwind, which is satisfactory for most problems. The second order and Osher options fail to work on NPS's SGI R8000 but this is being corrected with an update at the time of this writing. The last option is central differencing. The option diverges when used with finely defined meshes but the program allows the user to modify the degree of incorporation with the upwind. A 0.3 initial value of blending works with most grid patterns, while complex three dimensional problems require a more robust 0.5 mixture. The user manual does not give an example. The following example command for a turbulent case is offered to assist follow on researchers:

S_SCHEME UPWIND RHO K D

S_SCHEME CENTRAL U V

S_BLENDING 0.3 U V

All input properties are in metric dimensions. The time is specified by a start and stop time in seconds. The time increment for steps is specified by imputing the number of

twenty steps will yield a 0.1 second step increment. An eighty steps per vortex shedding period is a rough refinement for steady flow simulations.

The program has the ability to input polynomial and sine or cosine functions, which uses radians for their units vice degrees, for inputs. The program limits combinations to only two functions for any single parameter. The use of the spline feature is a substitute manner of input which allows the user to create more complete situations but it is limited to one hundred input points. By using the restart feature, a user can sequentially run any desired length of problem and effectively create an endless spline. Testing shows no loss of accuracy in computations by using a restarted spline.

The code allows the operator several options for output. By using the "PRINTF WALLS" command in the output section, the Yplus values of the wall will be listed in the output file. A value of approximately eleven or less indicates the Low-Re model should be used for turbulent models. Through the use of external Fortran programs, a user can summarize and collect the force data for additional analysis. This investigation uses Fortran and MATLAB programs to produce the force coefficient curves found in the Appendix.

The computer code is mainly used for other applications where the minimum relative pressure is not negative. This is applicable for interior flows, however, this is not true for exterior flows on bluff bodies. The minimum pressure must be modified in the output section of the program to include the following command to obtain correct results:

P_FORCE ON PMIN = -1E+05

IV. DISCUSSION OF RESULTS

A. INTRODUCTION

The numerical experiments are carried out through the use of a Silicon Graphics R8000 computer with a two gigabyte hard drive. The investigation uses the CFD-GEOM program as the grid generator and the CFD-ACE program as the equation solver. The code is relatively new and has very few papers describing the results of previous work. Therefore, the investigation starts with low steady flow ($Re < 500$) trails to verify the laminar capabilities. This is followed by a high flow case ($Re = 5 \times 10^4$) to test the turbulent features of the program. An oscillating flow case of $\beta = 1,000$ and $K = 20$ is investigated for its sensitivity to variable code parameters followed by a comparison of various β and K cases with historical laboratory experiments.

B. LOW FLOW VERIFICATION

Low flow verification is performed on two types of cylinders; square and round. The first testing is perform on a square cylinder at $Re = 400$ for the purpose of familiarization and visualization. A 0.01 m block is generated on a grid and subjected to a 0.04 m/s uniform steady flow. The results show a Karman Street with no imputed disturbance as seen in Figure 2.

The round cylinder is subjected to the same conditions but it generates two symmetric downstream vortices as seen in Figure 3. The vortices become 1 diameter in length at approximately 1.5 diameters of flow and then expand lengthwise and in magnitude for the remainder of the testing. This result matches laboratory experiments for non-disturbed cases. If perturbed, a Karman Street forms. The geometry of the square cylinder creates enough discontinuities at the corners so that no artificial disturbance is necessary for that case.

A simulated disturbance of a ramped 25 % increase and decrease in steady flow rate at the top half of the cylinder and proportionally the same amount of decrease and increase at the bottom half is added to create a cross flow on the formed vortices. It is timed to start at 1.5 diameters of flow for 1 diameter of flow. The lower the percentage, the longer the

disturbance time has to run to obtain the desired cross flow condition. This creates a Karman Street, as shown in Figure 4. Table 1 shows a comparison of the experimental and historical results. The Strouhal number and the force coefficient do not compare favorably at $Re = 100$. However, the testing does show an improving trend for both, with increasing speeds of flow. This test indicates that the model does not simulate properly the initiation and magnitude of vortices in the near wall region, but as the flow increases, which lessens the importance of these effects, the results improve.

Table 1. Comparison of Experimental and Historical In-Line Force Coefficients and Strouhal Numbers at Low Reynolds Numbers

Re	C_{IL}		Strouhal Number	
	<u>Experimental</u>	<u>Historical</u>	<u>Experimental</u>	<u>Historical</u>
100	1.07	1.8	0.13	0.165
200	1.0	1.4	0.14	0.18
400	1.1	1.2	0.16	0.19

C. HIGH FLOW VERIFICATION

Previous testing (Hufford 1995) shows the model to be reasonably accurate for steady flow about a square cylinder. However, the area of interest for this investigation is a circular cylinder. A single test at $Re = 5 \times 10^4$ is conducted with a turbulence level of 3 percent, Euler temporal differencing, central spacial differencing and, a 1/400 time interval to try to obtain approximately 80 steps per vortex separation. This yielded a $C_{IL} = 0.95$ which compares favorably to the historical value of 1.2. For two cycles, a Strouhal number of 0.24 is obtained which compares to a historical value of 0.23. Based on this result and the low Re testing, the model is found to sufficiently accurate to examine oscillatory flows at higher Re numbers.

D. OSCILLATING FLOWS

The baseline grid used for all of the testing of oscillating flow is a 1 meter by 1 meter square with a 0.05 meter diameter circular cylinder positioned in the center. There are 65 equally spaced mesh points on each of the outer boundaries while 130 points, with a .975 exponential spacing, are located in the axially direction. This creates 8,256 cells in each quadrant for a total of 33,024 for the model. This combination is used to generate cells that are half as long in the radial direction as their length along the cylinder wall while achieving nearly square cells near the boundary to better capture the pressure and velocity gradients by the wall. The resulting structure can be seen in Figure 1.

The initial trial run uses a $K - \epsilon$ turbulence model and SIMPLEC algorithm. The time interval is 0.02 seconds with a first order upwind spatial differencing scheme and euler temporal differencing scheme. The turbulence level at the boundary is 3 % with a corresponding turbulence length scale. No disturbances are required to generate the lift crisis for oscillating flow cases and therefore not used. Twenty iterations are performed at each time step. All runs use $\beta = 1,000$ and $K = 20$ for a $Re = 20,000$. This flow velocity combined with the grid geometry and time intervals creates a Neumann number of 0.5 at the boundaries of the grid area.

The code's variable parameters are tested for their sensitivity and the results are summarized in Table 2. The initial baseline model obtains a C_{IL} of 1.1 compared to a historical maximum peak value of 1.9.

Table 2. Sensitivity of Parameters on the C_{IL}

<u>Parameter</u>	<u>Factor of Change</u>	<u>Relative Percent</u>		
		<u>of Change</u>	<u>Original</u>	<u>New</u>
Time Interval	0.02 to .01	0.5	1.33	1.34
Time Interval	0.02 to .0025	0.5	1.33	1.34
Turbulence Level	3% to 10%	2.4	1.80	1.85
Model Type	K - ϵ to RNG	6.8	1.09	1.22
Model Type	K - ϵ to Low Re	12.3	1.09	1.33
Spatial Differencing	Upwind to Central	9.7	1.33	1.52
Temporal Differencing	Euler to Crank Nicholson	-4.1	1.33	1.25
Turbulence Length Scale	0.0025 to 0.0045	2.0	1.09	1.13
Number of Iterations per step	40 to 20	0.0	1.22	1.22
Number of Iterations Step per Step	20 to 10	0.0	1.22	1.22
Number of Iterations per Step	20 to 5	-5.1	1.22	1.22

The optimum combination uses 10 iterations per step with a 0.02 time interval per step which does not impact the results but reduces the time to run the problem by over 60 % compared to the original model. The temporal differencing, turbulence level and, length scale all remain the same as the baseline model. The simulation is altered to have a Low Re turbulence model and central spatial differencing. This combination increases the maximum observed C_{IL} to 1.5. Additional testing shows the lift crisis significantly increases the peak C_{IL} from 1.5 to 1.8 which may of contributed to the low value for the initial model. Figure 5 shows the visualization of one cycle of flow.

The grid size definition is tested next by doubling the number of boundary points creating a 133,644 cell grid. The grid refinement is able to capture more of the magnitude of the vortices than the course grid which results in a 1.7 C_{IL} prior to lift crisis and a 1.8 after the crises. However, this increase in grid definition slows the computer by over 400 % compared to the basic line model and does not provide additional improvement in force coefficients after the lift crisis.

The optimum model is next tested at various β and K combinations that correspond to previous testing for comparison (Sarpkaya 1976). Figure 5 - 34 show the in-line and transverse forces for each combination and are summarized in Table 3.

Table 3. Oscillating Flow In-Line Force Coefficient Results

K	$\beta = 1,000$		$\beta = 2,000$		$\beta = 3,100$	
	<u>Computer</u>	<u>Historical</u>	<u>Computer</u>	<u>Historical</u>	<u>Computer</u>	<u>Historical</u>
8	2.6	2.4	2.45	2.5	2.45	2.4
12	2.25	2.3	1.72	2	1.7	1.45
20	1.8	1.95	1.15	1.3	1.1	1.0
25	1.3	1.6	0.95	1.15	1.0	0.9
35	1	1.35	0.83	0.85	0.9	0.85

The following observations are made:

1. The $\beta = 2,000$ data acted more like a higher β number and particularly in the mid K flows.
2. The K=8 and K=35 cases usually yielded best similarity to the historical data. The K=8 case may be due to the flow being less complex than K=12 case. At high Ks, a plateau is reached where the C_{IL} is more relatively constant. The code is able to capture most of the vortex strength and, therefore, the results tend to be more accurate in the region of higher K values.

3. The dissipation of visualized vortices and their strengths are higher than nature or previously used codes. This may be the cause for the lower force coefficients.
4. The $\beta = 1000$ has a longer time to the lift crises which may be due to lower U_M values.

A view of the vortices during one oscillation for $\beta = 1,000$ and $K = 8$ shows in Figures 35 and 36 the formation, detachment, and the reentry into the wall region on flow reversal. Figures 37 through 40 show the start of a transverse street for the $\beta = 1,000$ and $K = 12$ case. Figures 41 through 44 show the return of the normal oscillation pattern for the $\beta = 1,000$ and $K = 20$. Figures 45 and 46 for $\beta = 2,000$ and $K = 20$ begin to show the effect of higher flows where each half cycle acts like an impulsive start and forms symmetric vortices. This effect can be seen more clearly in a series of views for $\beta = 3,100$ and $K = 35$ shown in Figures 47 through 50 but the vortices are more elongated and do not linger near the cylinder because of the higher U_M .

Overall, the trend of the data is well predicted for the pure oscillatory case with no steady mean flow. The program has limitations in fully capturing the generated forces and dissipation but does allow a look at flow levels not previously tested on a non-super computer.

V. CONCLUSIONS

The investigation reported here warranted the following conclusions:

1. Finite differencing formulations of the Favre Averaged Navier Stokes equations (FANS) can reasonably solve a wide range of Reynolds number flows, using a modified SIMPLE method.
2. The laminar flow model predicts the trend of Strouhal numbers but does not favorably predict low Reynolds number force coefficients. The comparability with historical values does improve with higher Reynolds number flows. The force coefficients correspond to higher Reynolds number conditions, but the Strouhal numbers correspond to the actual or lower flow conditions.
3. The numerical experiments with oscillating flows for β of 1,000, 2,000 and, 3,100 yield In-Line Force Coefficients in good agreement with those obtained experimentally.
4. The program does not fully capture vortex strengths and prematurely dissipates the vortices relative to previous investigations.
5. The numerical experiments presented herein can be performed on a non-super computer. The fact that numerical instabilities versus fluid dynamical instabilities have different and at times competing mathematical and computational demands necessitated a compromise in grid definition and time interval spacing. In spite of this, eight hours of computer run time were required to generate twenty seconds of true flow for most of the oscillatory cases.

APPENDIX

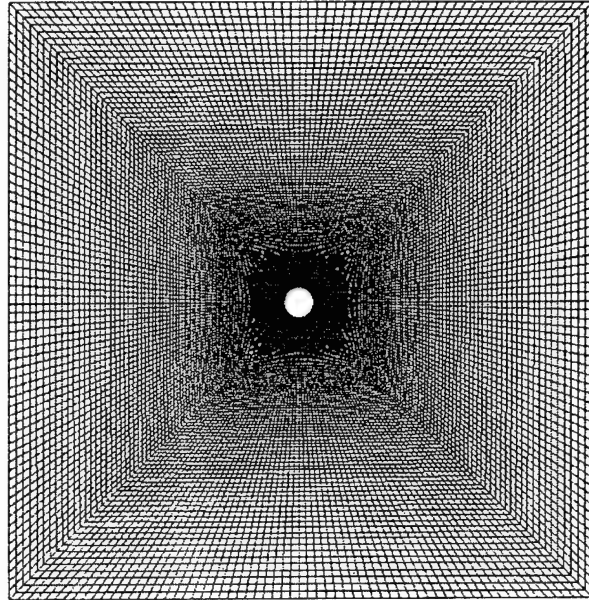


Figure 1. Grid in the Physical Domain

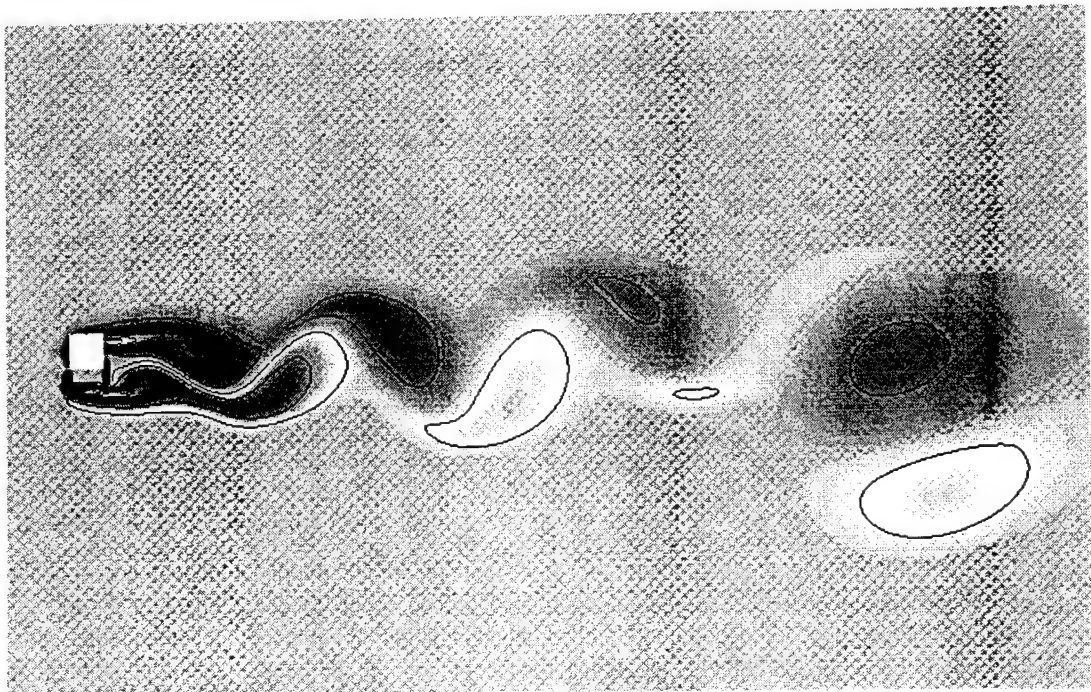


Figure 2. Flow About a Square Cylinder at $Re = 400$

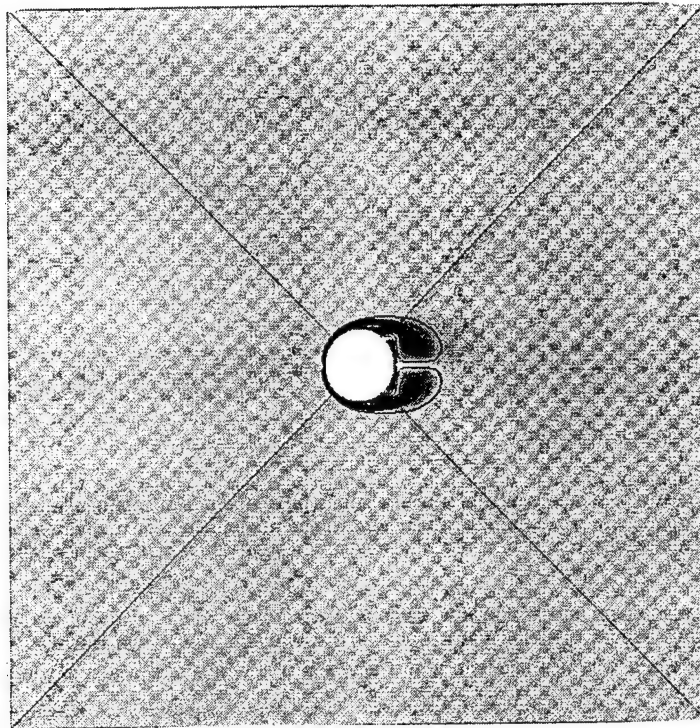


Figure 3. Flow About a Circular Cylinder at $Re = 400$

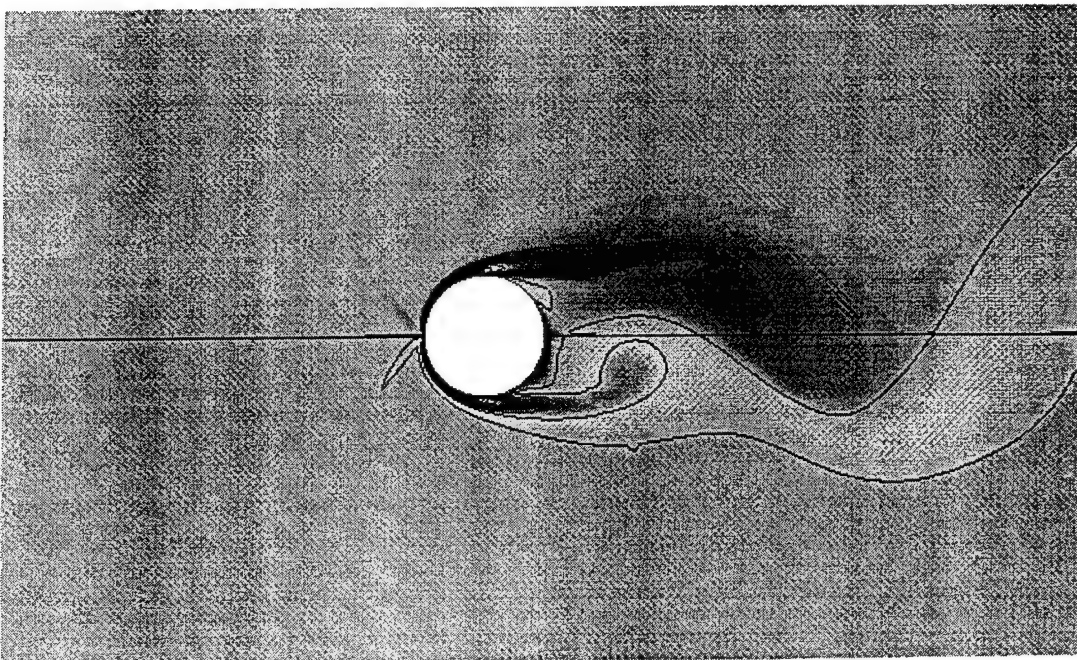


Figure 4. Flow About a Circular Cylinder at $Re = 400$

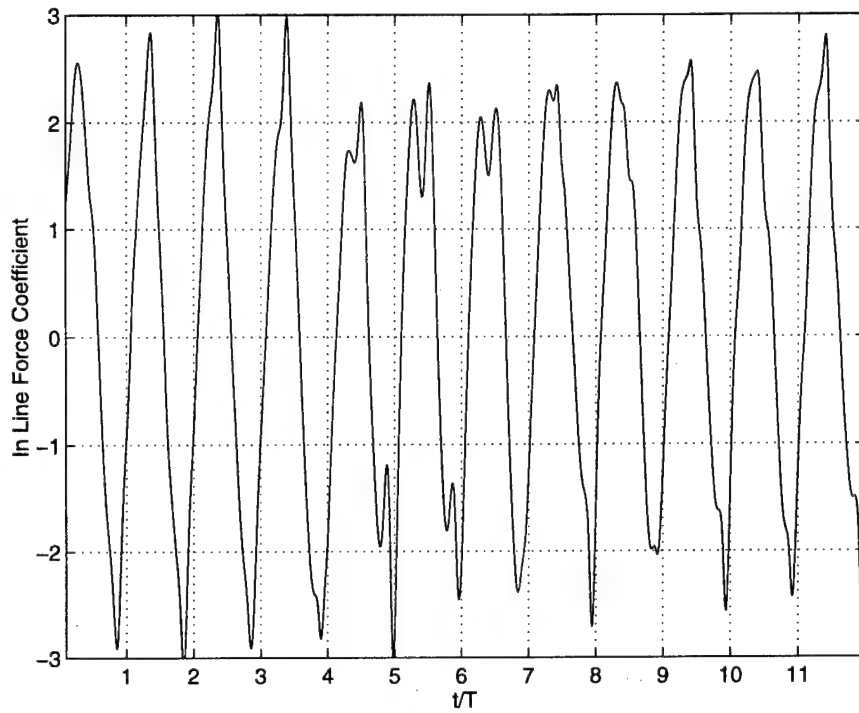


Figure 5. Inline Force Coefficient vs t/T , $\beta = 1,000$, $K=8$, $Re = 8,000$

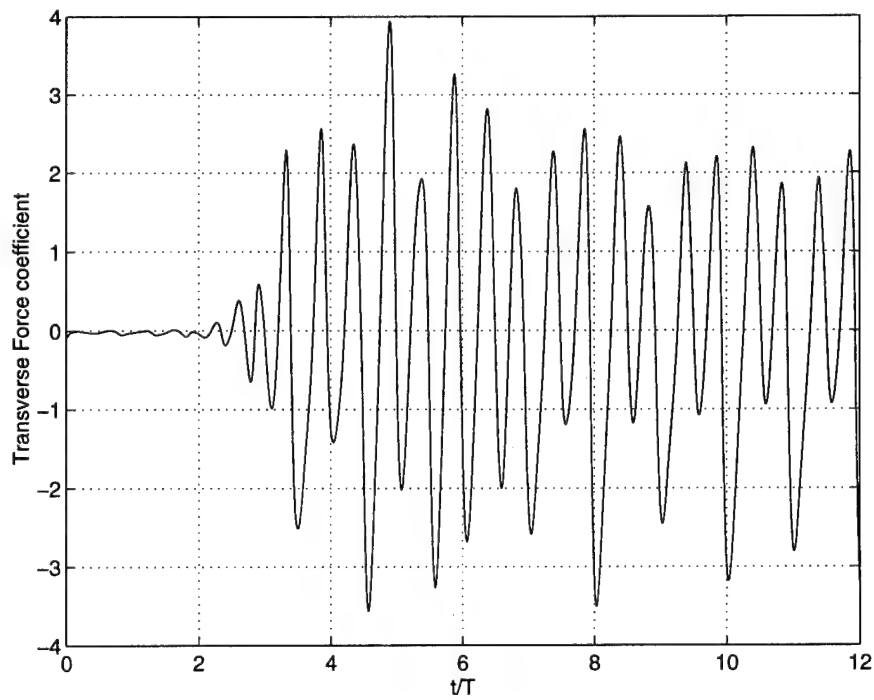


Figure 6. Transverse Force Coefficient vs t/T , $\beta= 1,000$, $K=8$, $Re = 8,000$

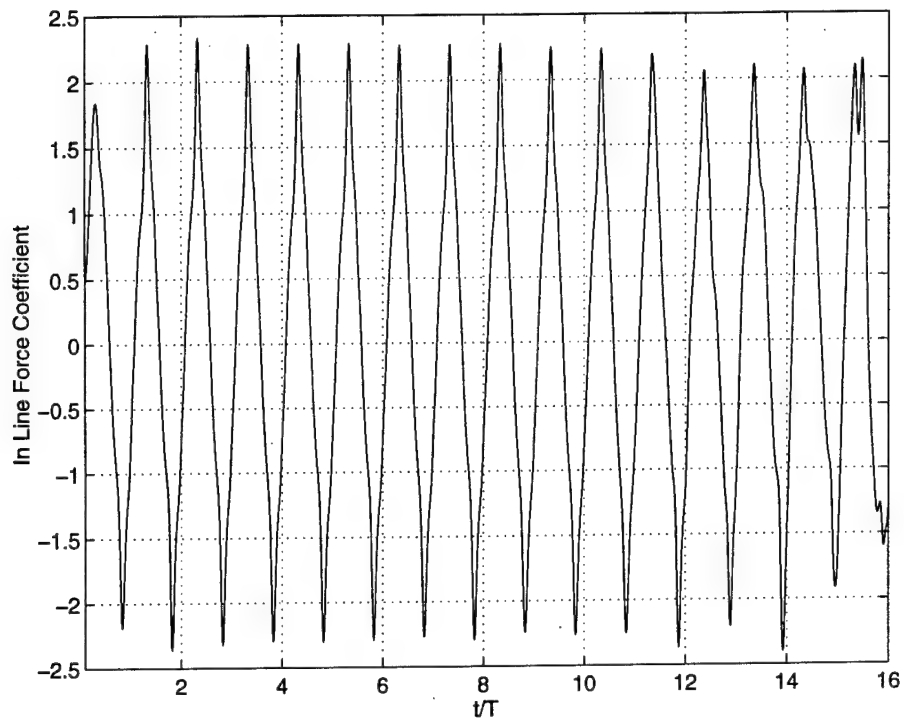


Figure 7. Inline Force Coefficient vs t/T , $\beta = 1,000$, $K = 12$, $Re = 12,000$

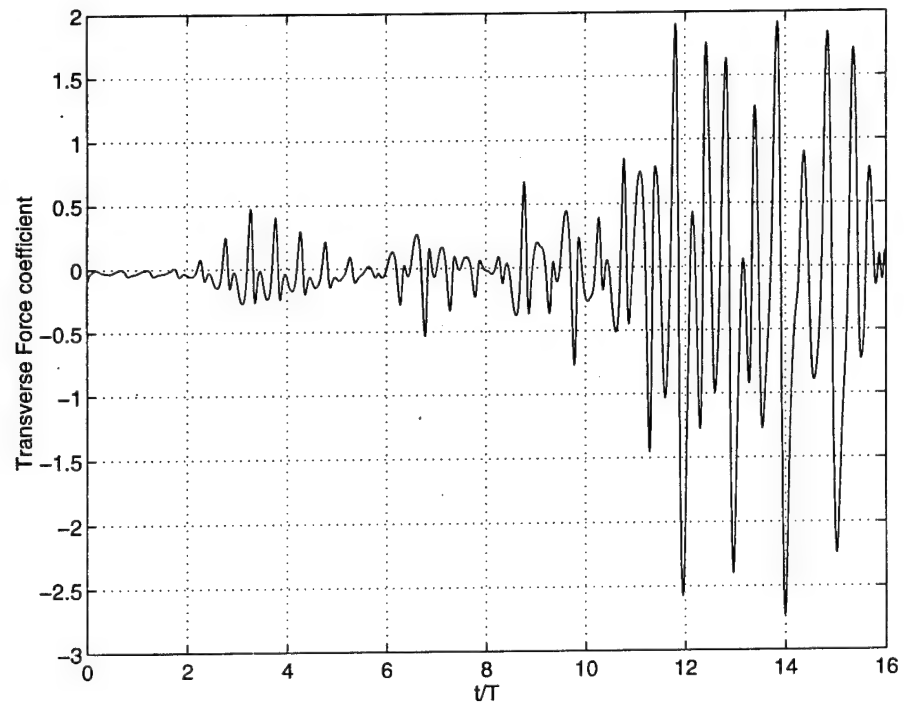


Figure 8. Transverse Force Coefficient vs t/T , $\beta = 1,000$, $K = 12$, $Re = 12,000$

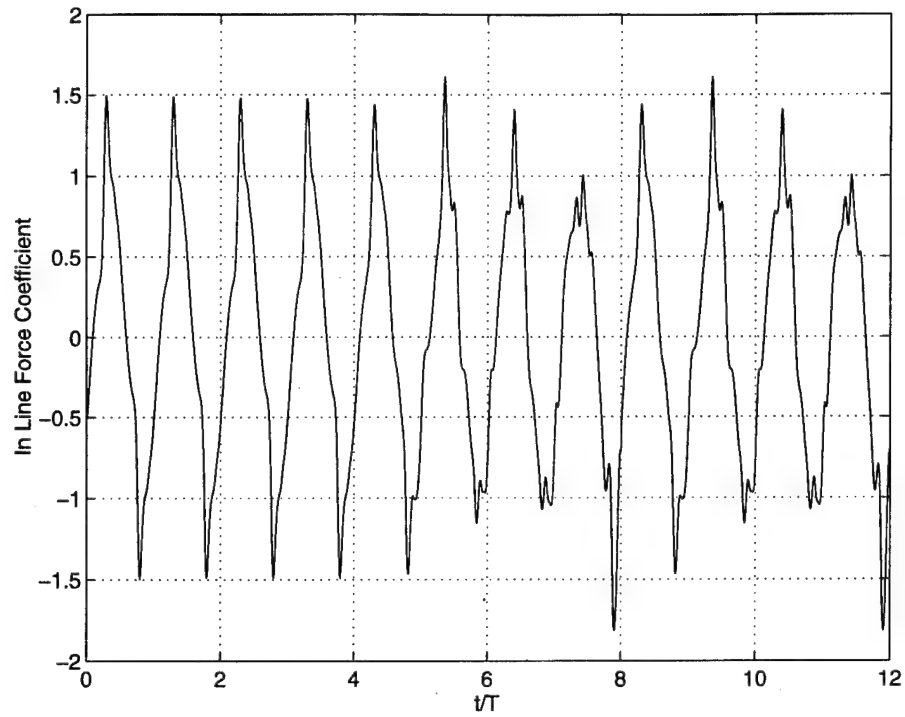


Figure 9. Inline Force Coefficient vs t/T , $\beta = 1,000$, $K=20$, $Re = 20,000$

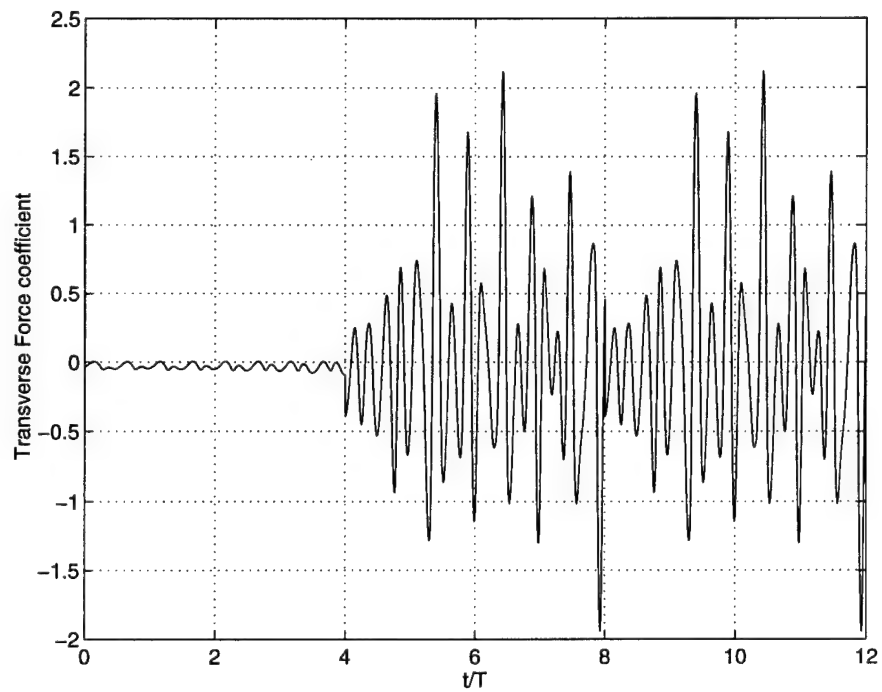


Figure 10. Transverse Force Coefficient vs t/T , $\beta = 1,000$, $K=20$, $Re = 20,000$

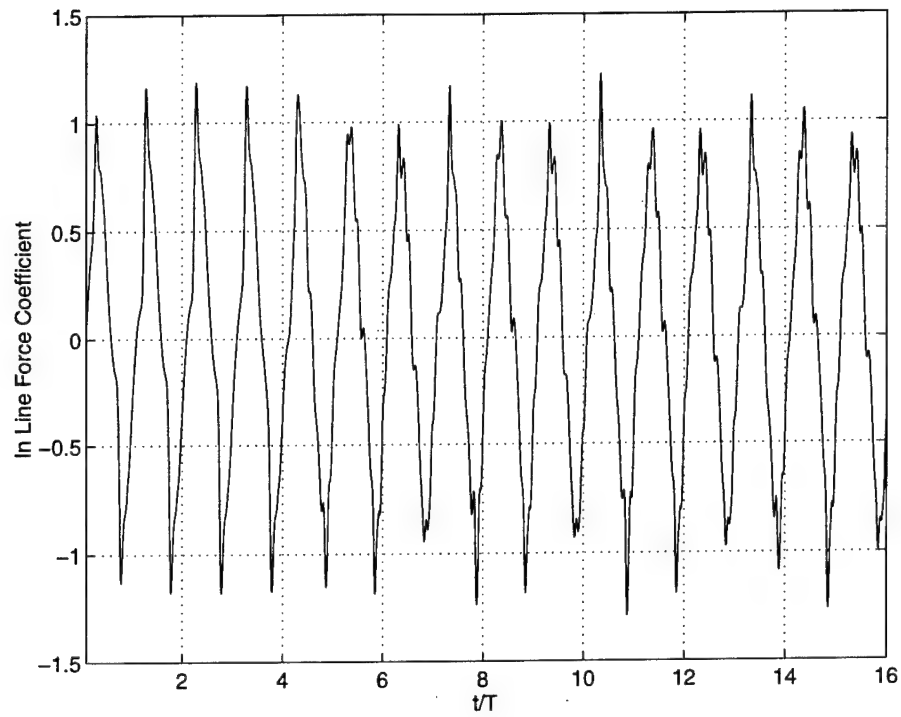


Figure 11. Inline Force Coefficient vs t/T , $\beta = 1,000$, $K = 25$, $Re = 25,000$

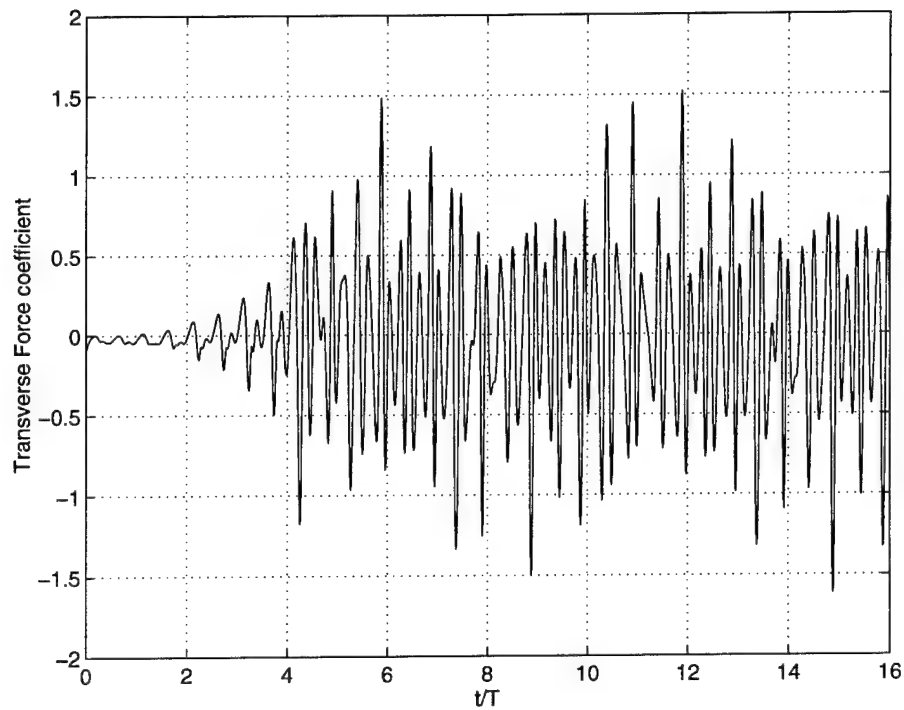


Figure 12. Transverse Force Coefficient vs t/T , $\beta = 1,000$, $K = 25$, $Re = 25,000$

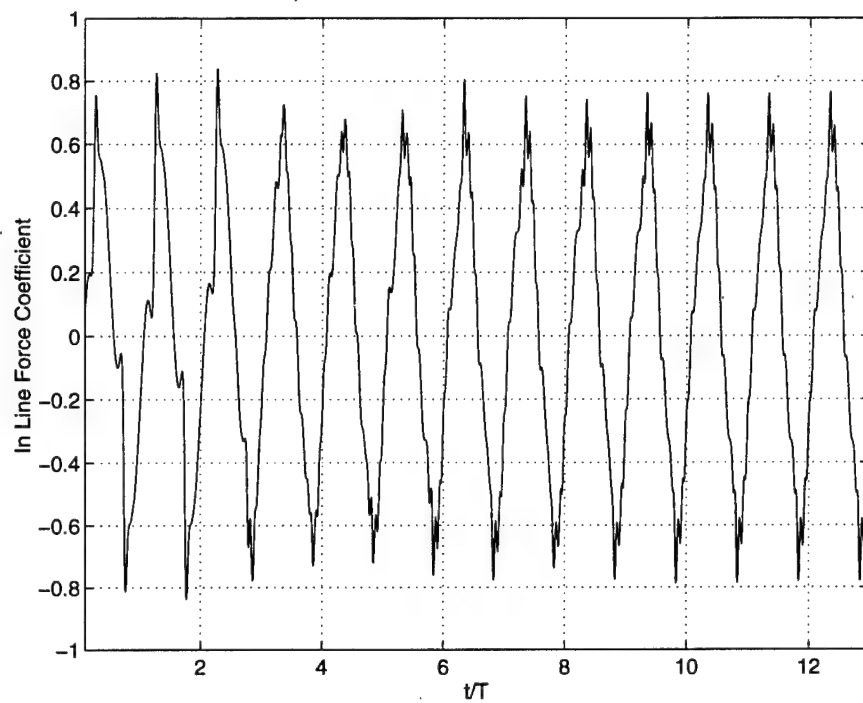


Figure 13. Inline Force Coefficient vs t/T , $\beta = 1,000$, $K = 35$, $Re = 35,000$

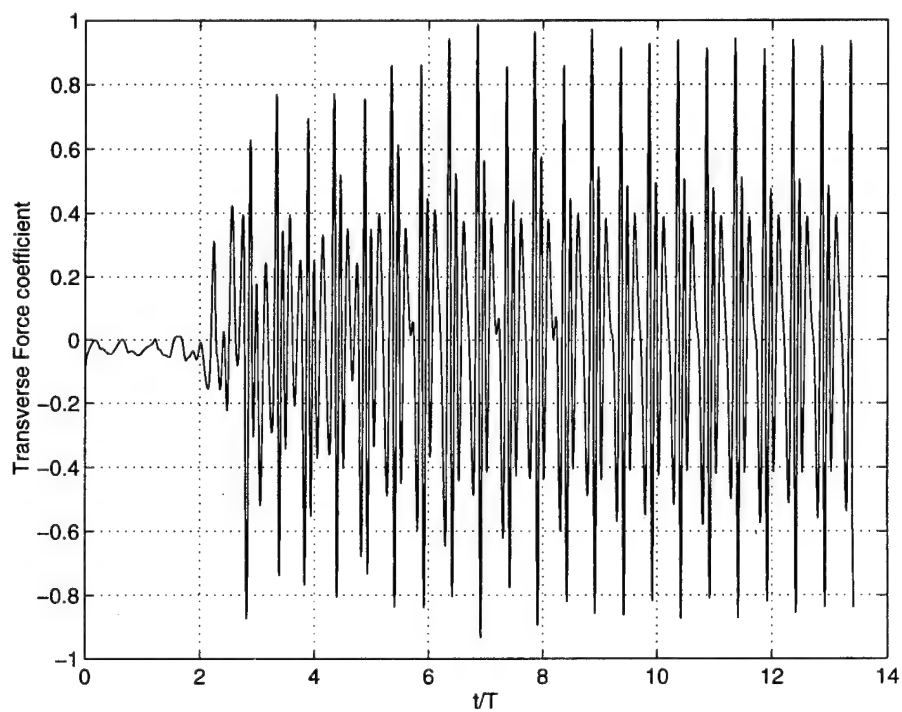


Figure 14. Transverse Force Coefficient vs t/T , $\beta = 1,000$, $K = 35$, $Re = 35,000$

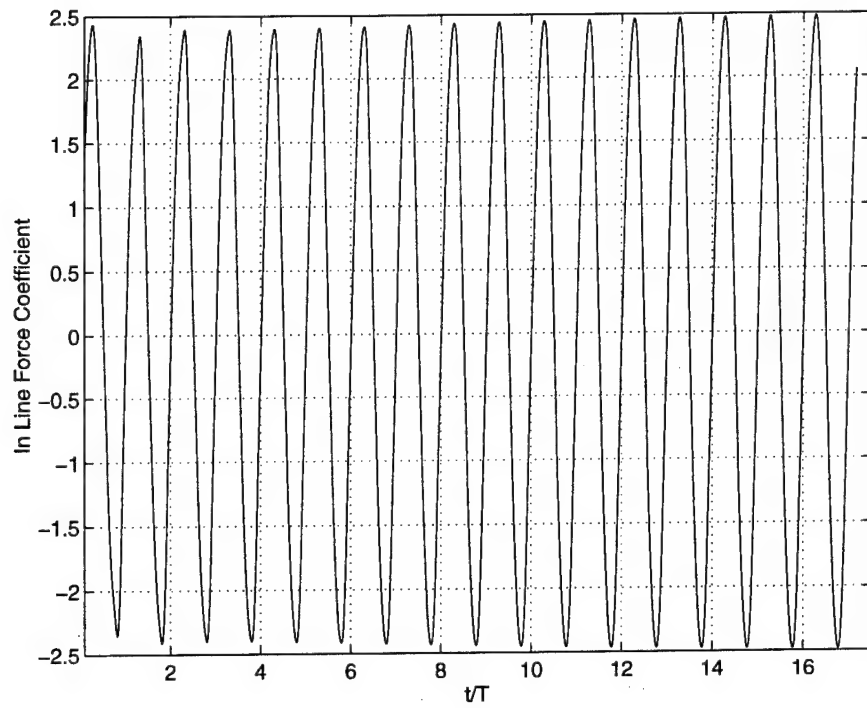


Figure 15. Inline Force Coefficient vs t/T , $\beta = 2,000$, $K = 8$, $Re = 16,000$

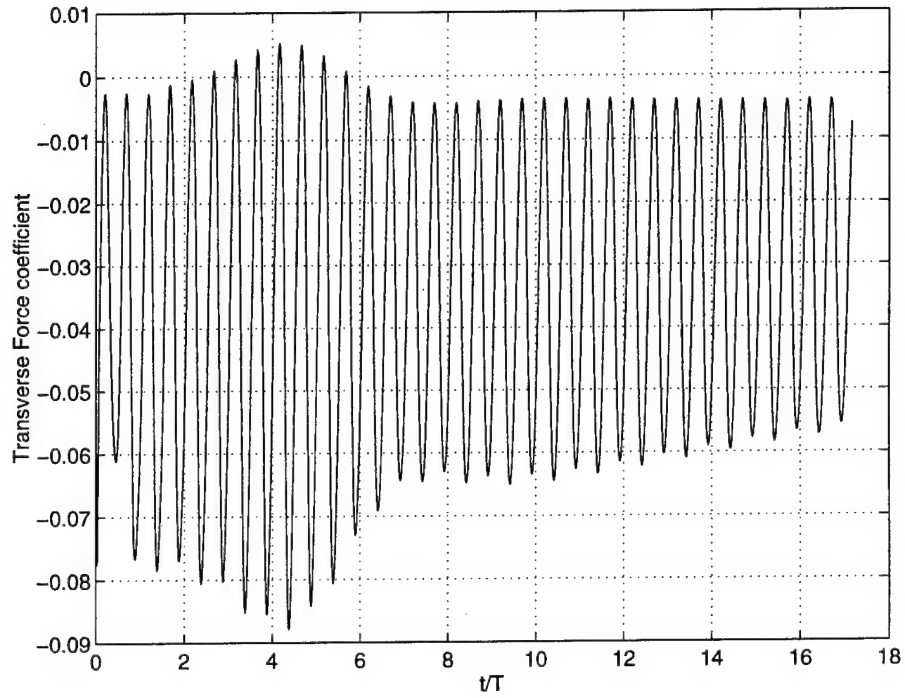


Figure 16. Transverse Force Coefficient vs t/T , $\beta = 2,000$, $K = 8$, $Re = 16,000$

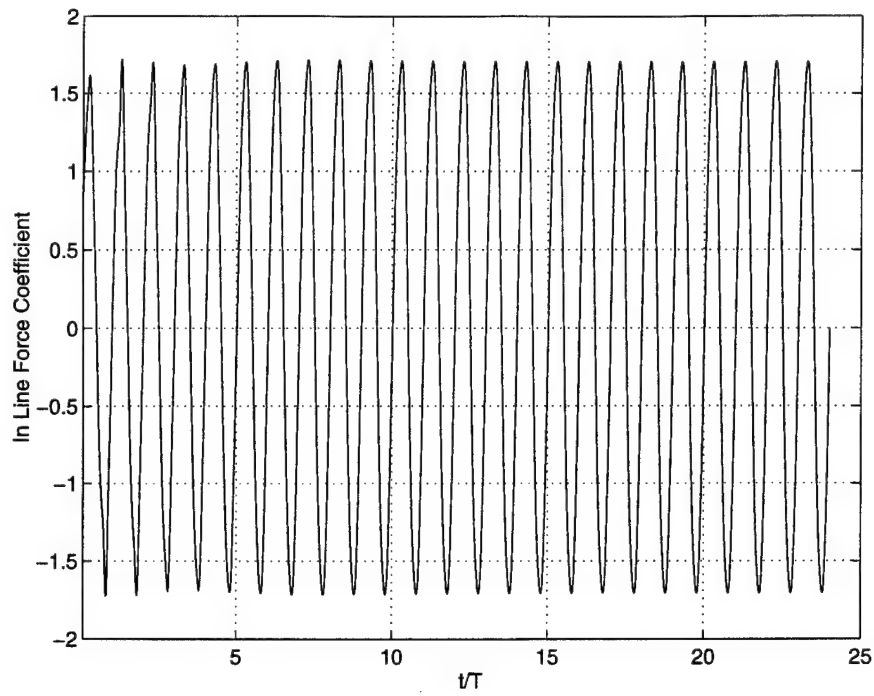


Figure 17. Inline Force Coefficient vs t/T , $\beta = 2,000$, $K = 12$, $Re = 24,000$

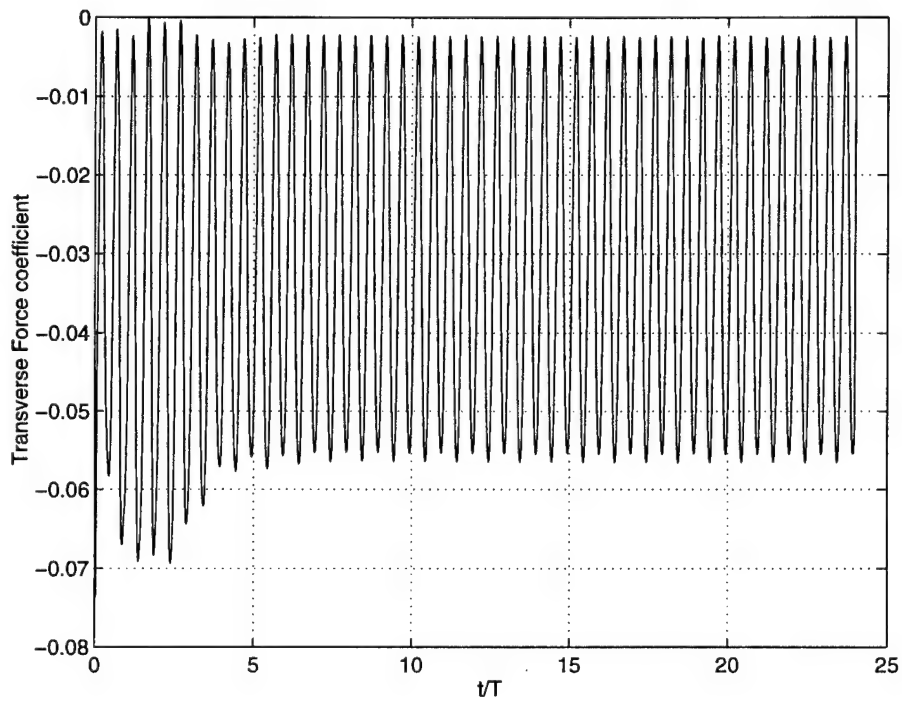


Figure 18. Transverse Force Coefficient vs t/T , $\beta = 2,000$, $K = 12$, $Re = 24,000$

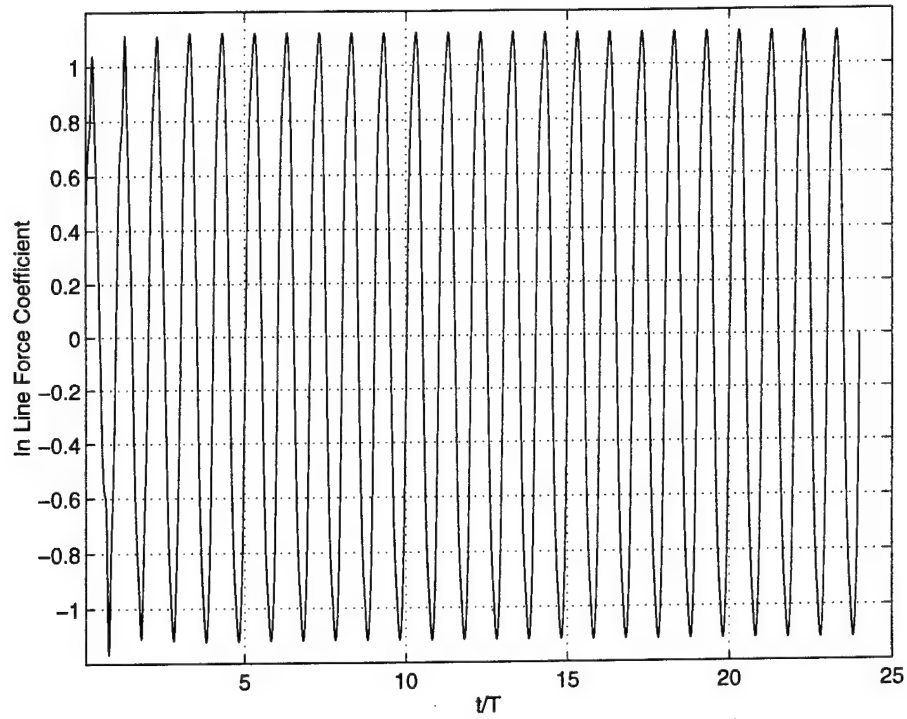


Figure 19. Inline Force Coefficient vs t/T , $\beta = 2,000$, $K = 20$, $Re = 40,000$

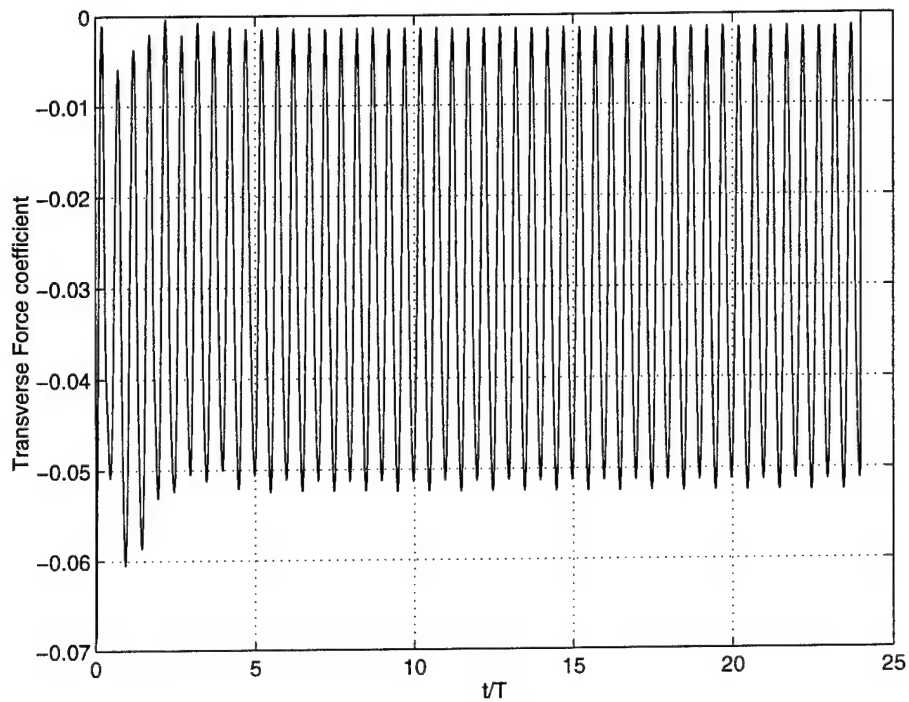


Figure 20. Transverse Force Coefficient vs t/T , $\beta = 2,000$, $K = 20$, $Re = 40,000$

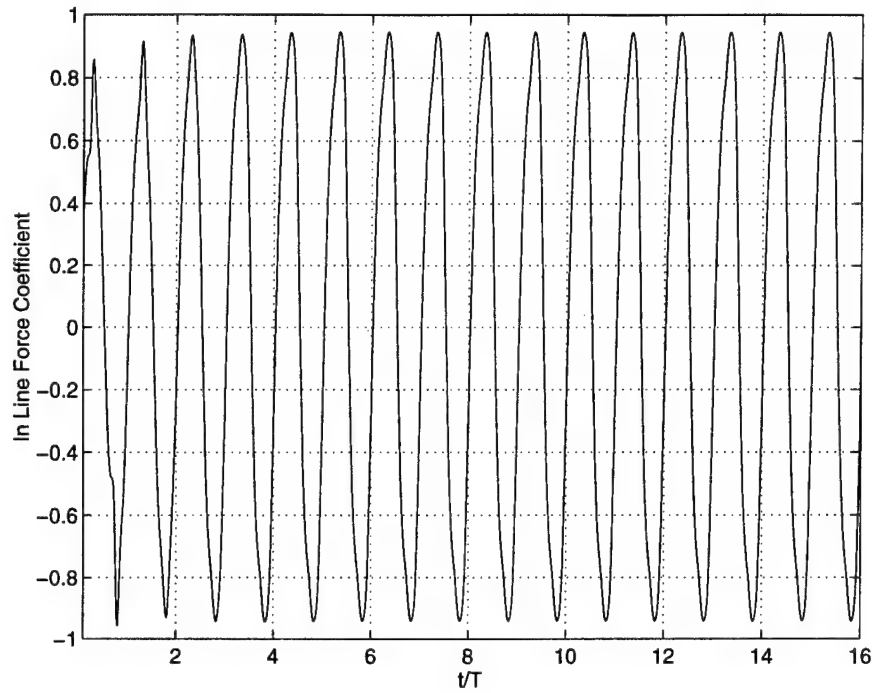


Figure 21. Inline Force Coefficient vs t/T , $\beta = 2,000$, $K = 25$, $Re = 50,000$

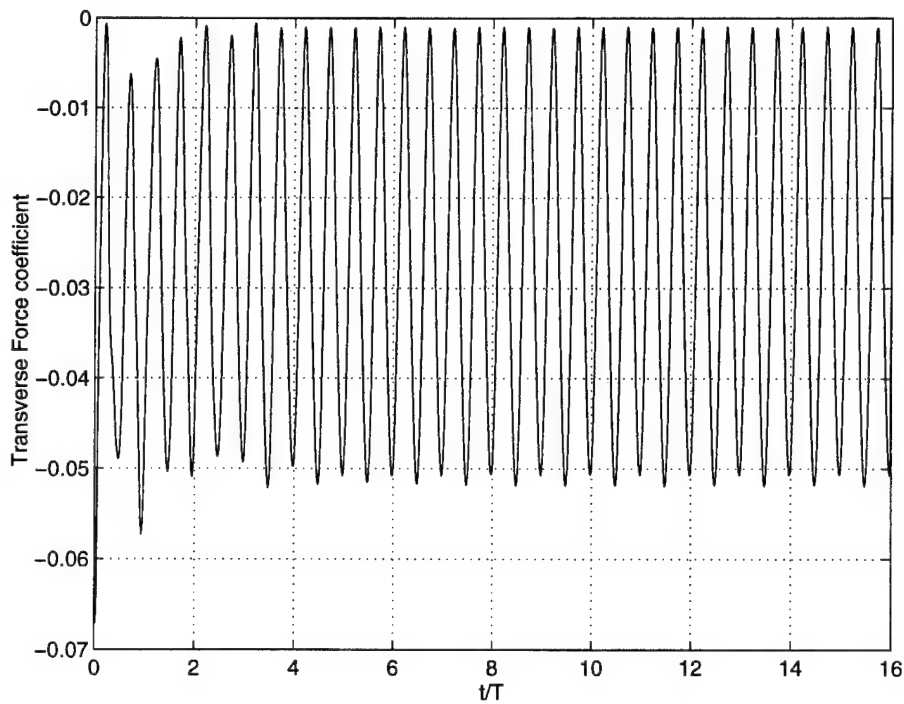


Figure 22. Transverse Force Coefficient vs t/T , $\beta = 2,000$, $K = 25$, $Re = 50,000$

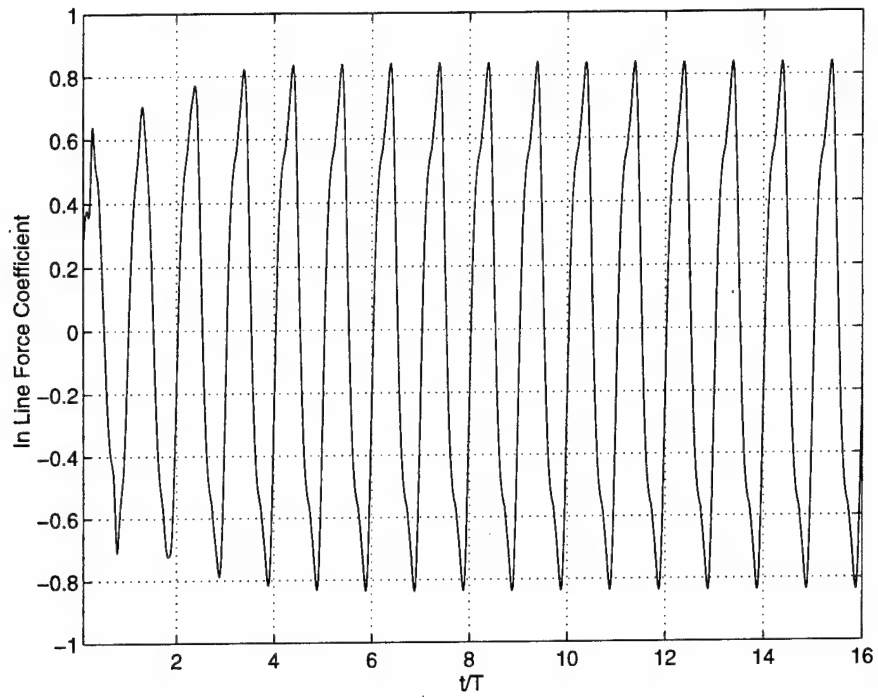


Figure 23. Inline Force Coefficient vs t/T , $\beta = 2,000$, $K = 35$, $Re = 70,000$

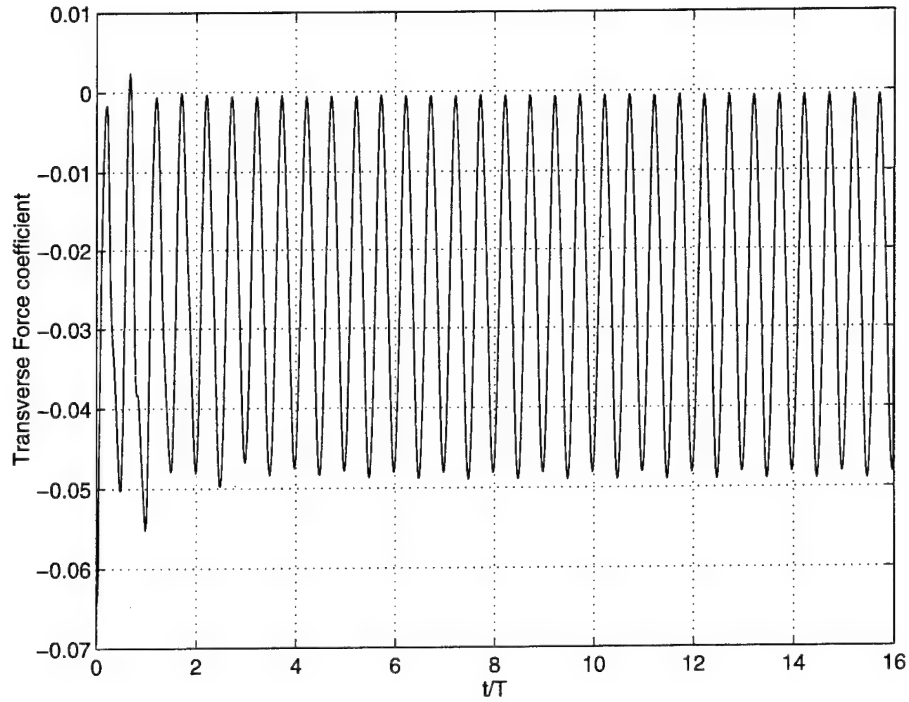


Figure 24. Transverse Force Coefficient vs t/T , $\beta = 2,000$, $K = 35$, $Re = 70,000$

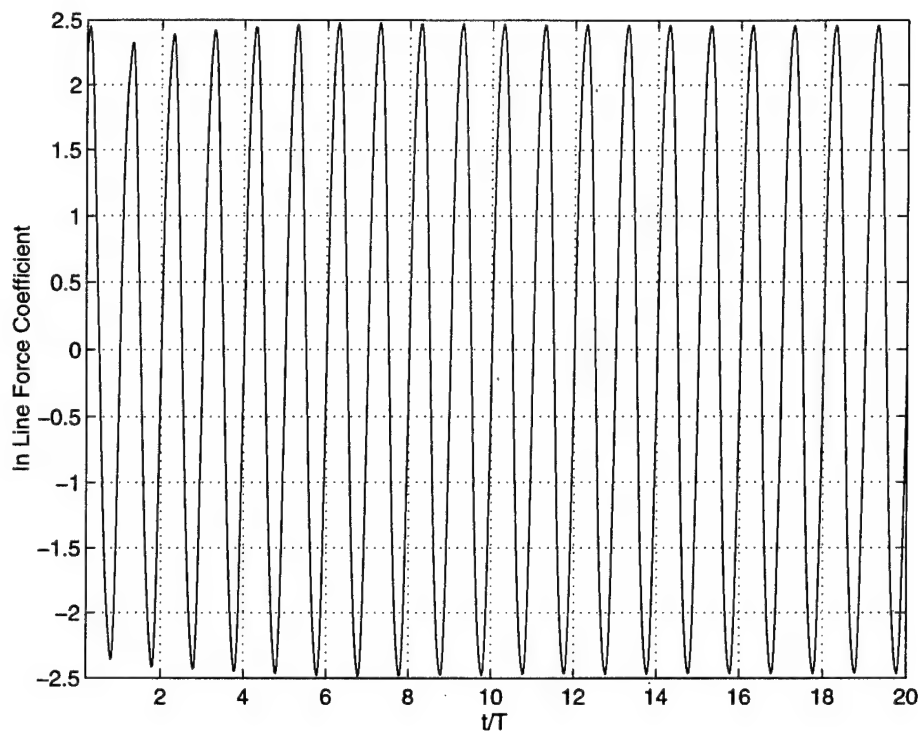


Figure 25. Inline Force Coefficient vs t/T , $\beta = 3,100$, $K = 8$, $Re = 24,800$

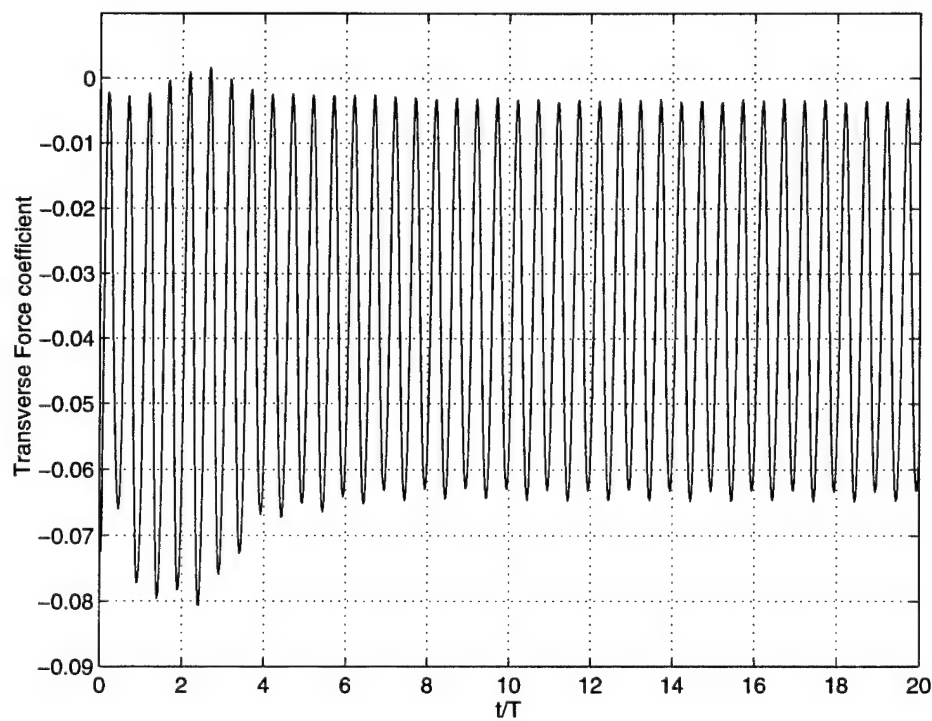


Figure 26. Transverse Force Coefficient vs t/T , $\beta = 3,100$, $K = 8$, $Re = 24,800$

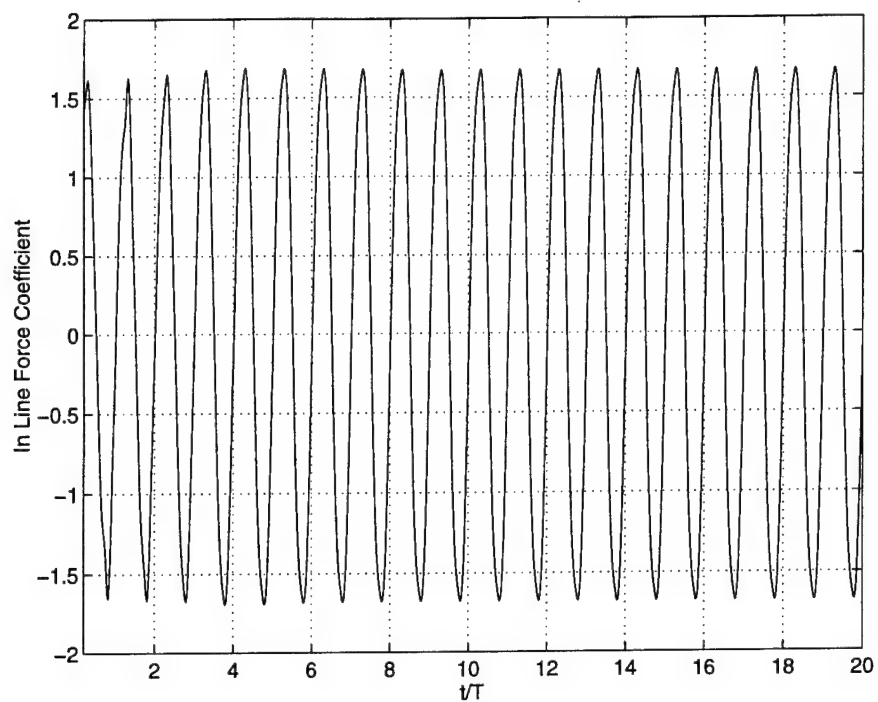


Figure 27. Inline Force Coefficient vs t/T , $\beta = 3,100$, $K = 12$, $Re = 37,200$

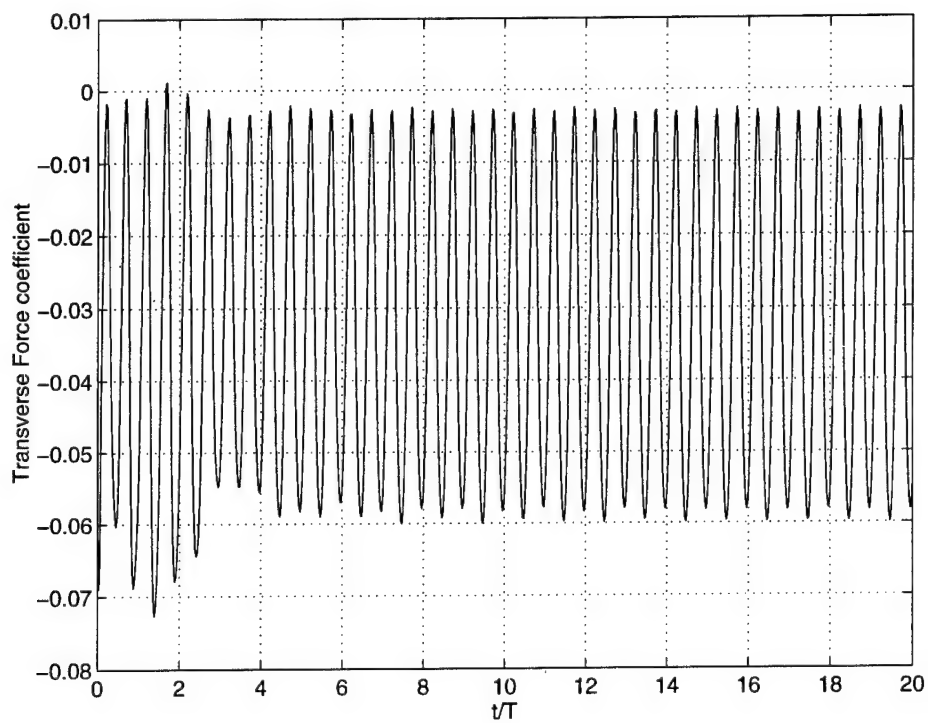


Figure 28. Transverse Force Coefficient vs t/T , $\beta = 3,100$, $K = 12$, $Re = 37,200$

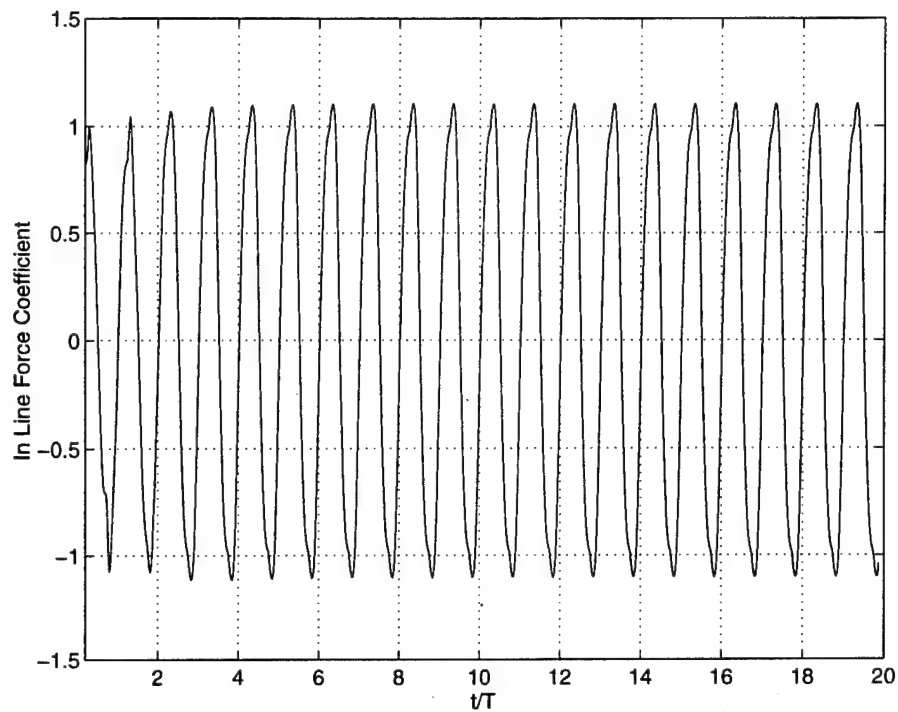


Figure 29. Inline Force Coefficient vs t/T , $\beta = 3,100$, $K = 20$, $Re = 62,000$

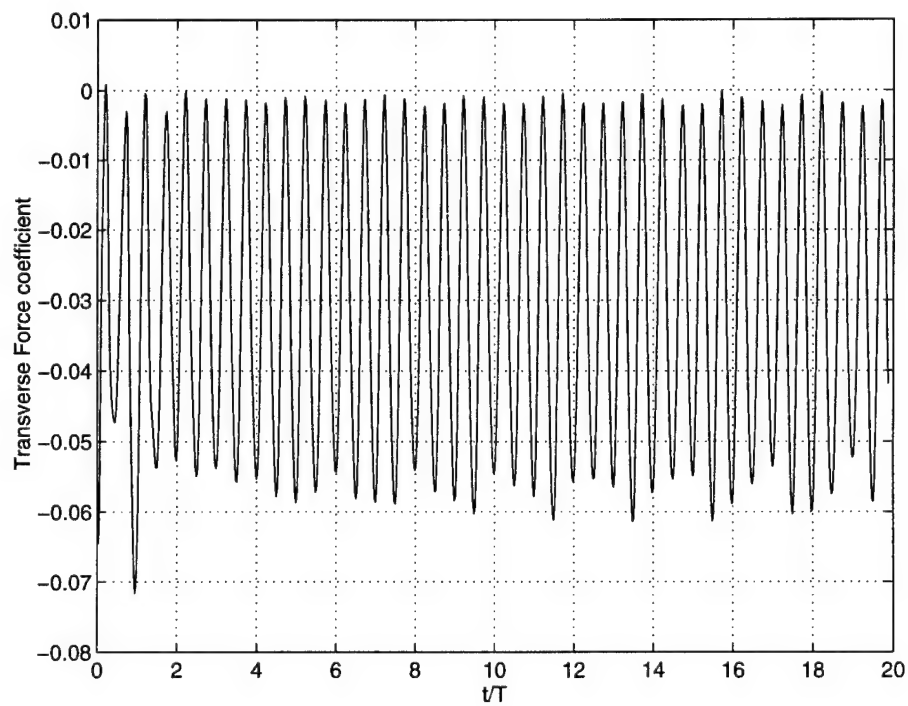


Figure 30. Transverse Force Coefficient vs t/T , $\beta = 3,100$, $K = 20$, $Re = 62,000$

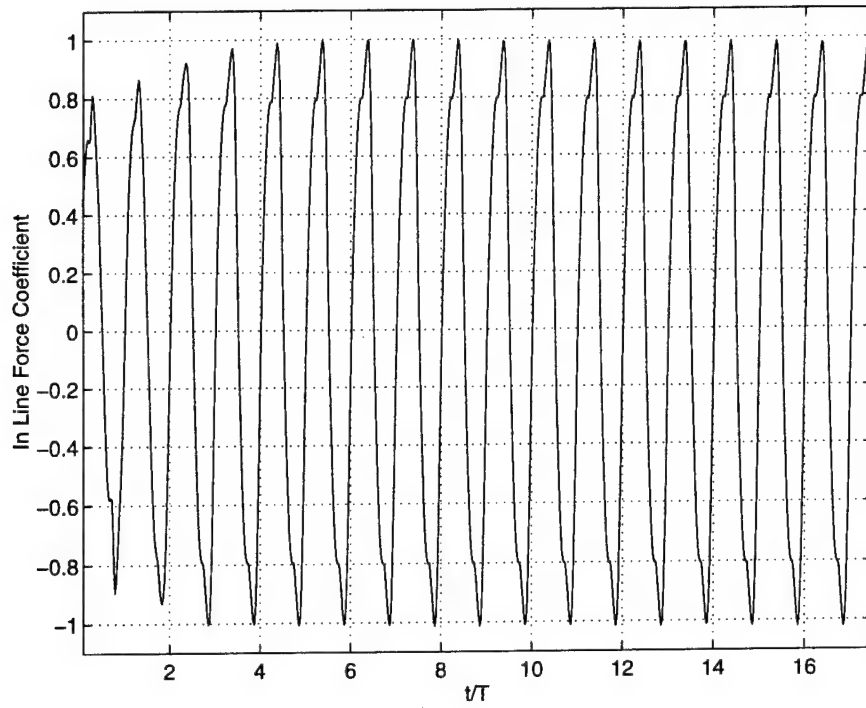


Figure 31. Inline Force Coefficient vs t/T , $\beta = 3,100$, $K = 25$, $Re = 77,500$

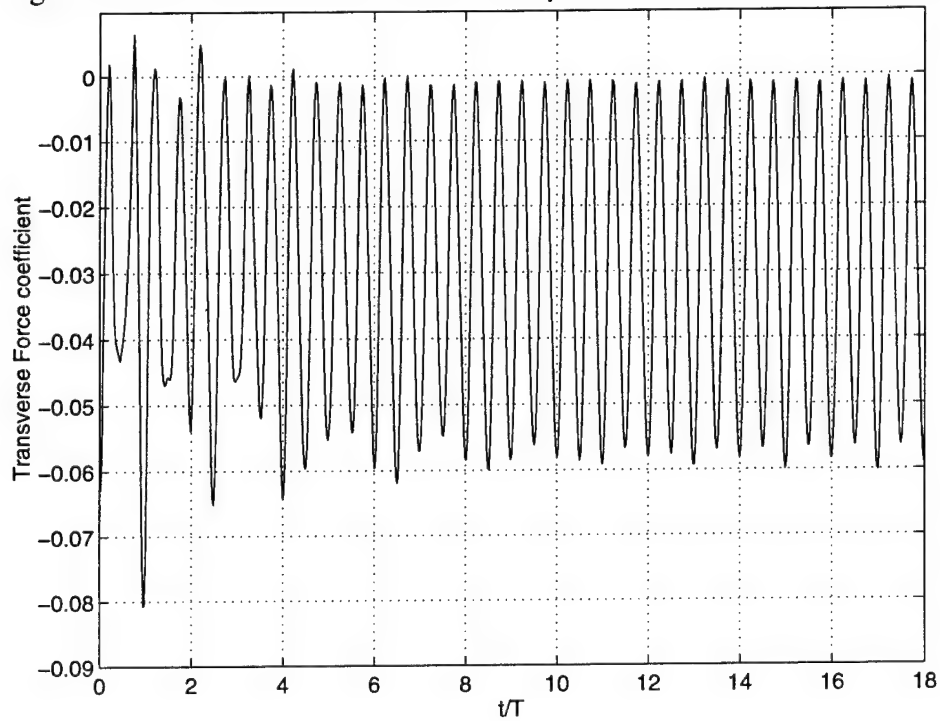


Figure 32. Transverse Force Coefficient vs t/T , $\beta = 3,100$, $K = 25$, $Re = 77,500$

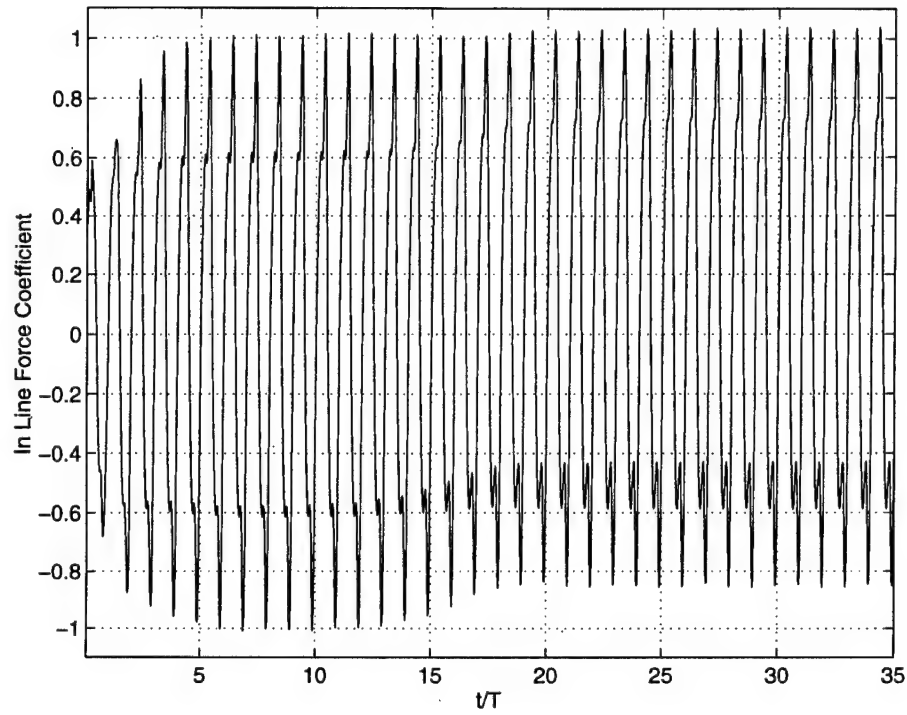


Figure 33. Inline Force Coefficient vs t/T , $\beta = 3,100$, $K = 35$, $Re = 108,500$

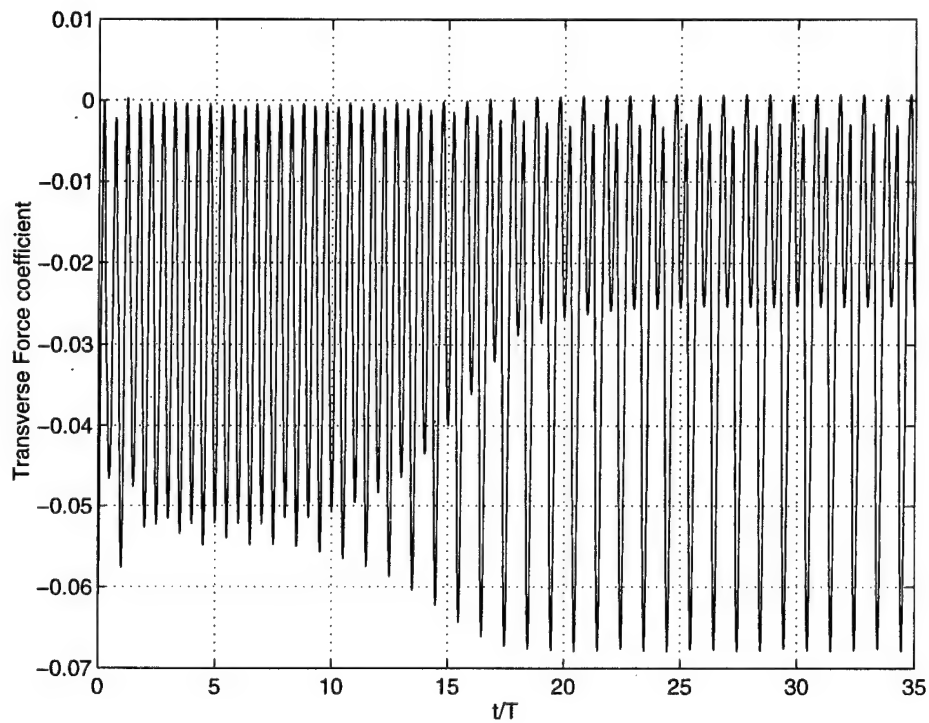


Figure 34. Transverse Force Coefficient vs t/T , $\beta = 3,100$, $K = 35$, $Re = 108,000$

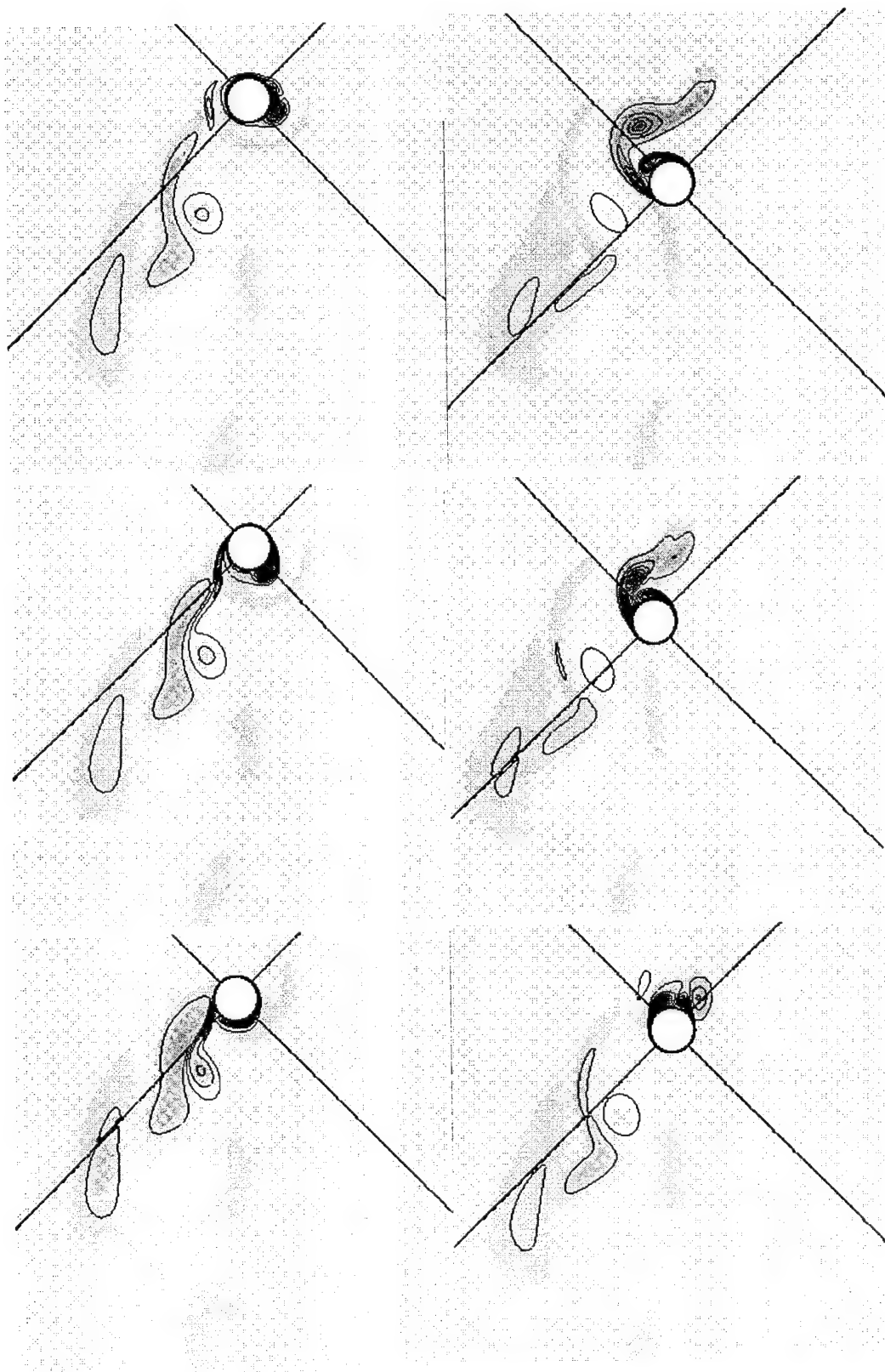


Figure 35. Vorticity Plot for an Oscillatory Flow About a Circular Cylinder at $\beta = 1000$, $K = 8$, $Re = 8,000$
(Steps 1 - 6 in Increments of 45 Degrees, Left to Right, Top to Bottom)

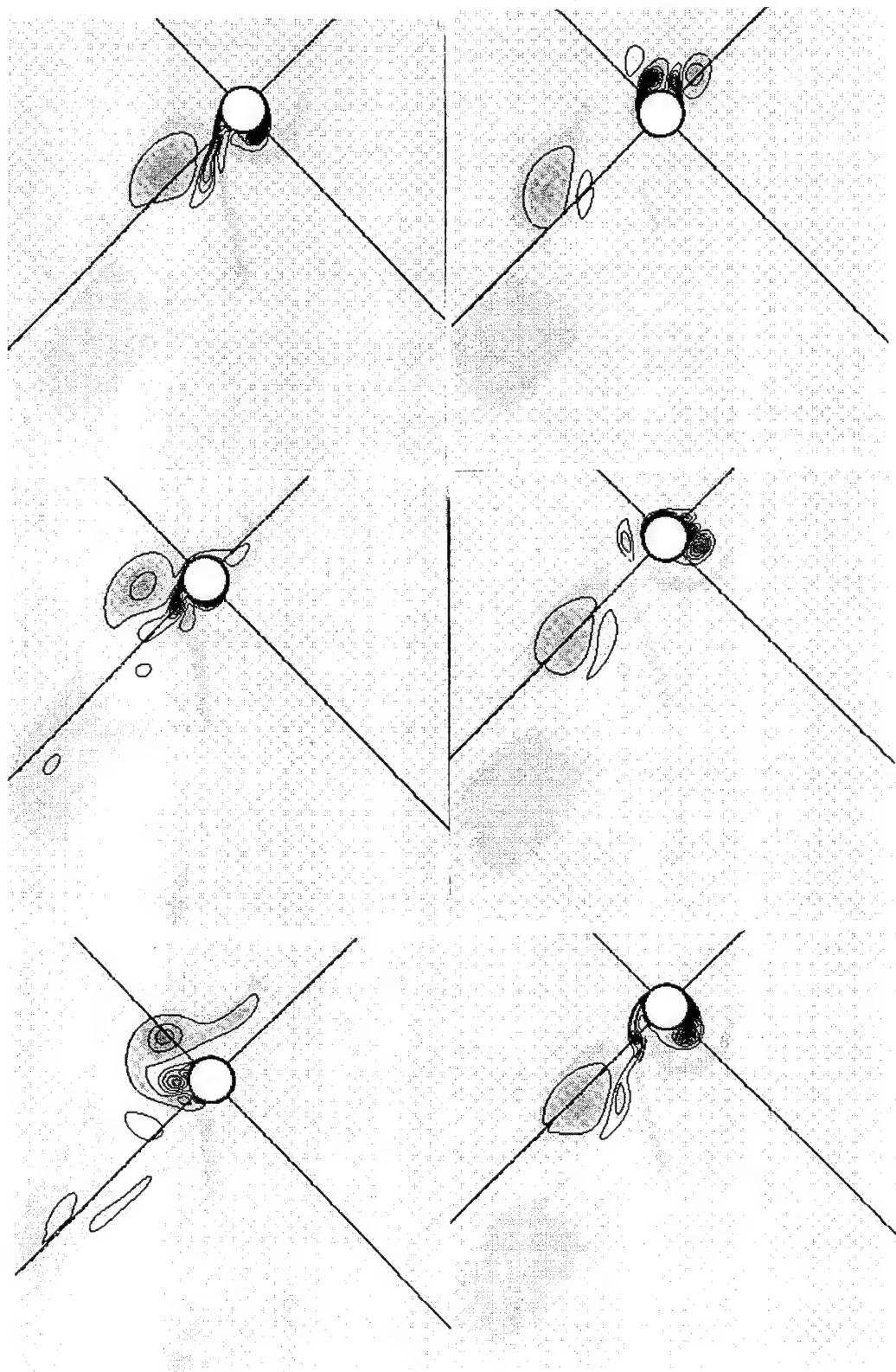


Figure 36. Vorticity Plot for an Oscillatory Flow About a Circular Cylinder at $\beta = 1000$, $K = 8$, $Re = 8,000$
(Steps 7 - 12 in Increments of 45 Degrees, Left to Right, Top to Bottom)

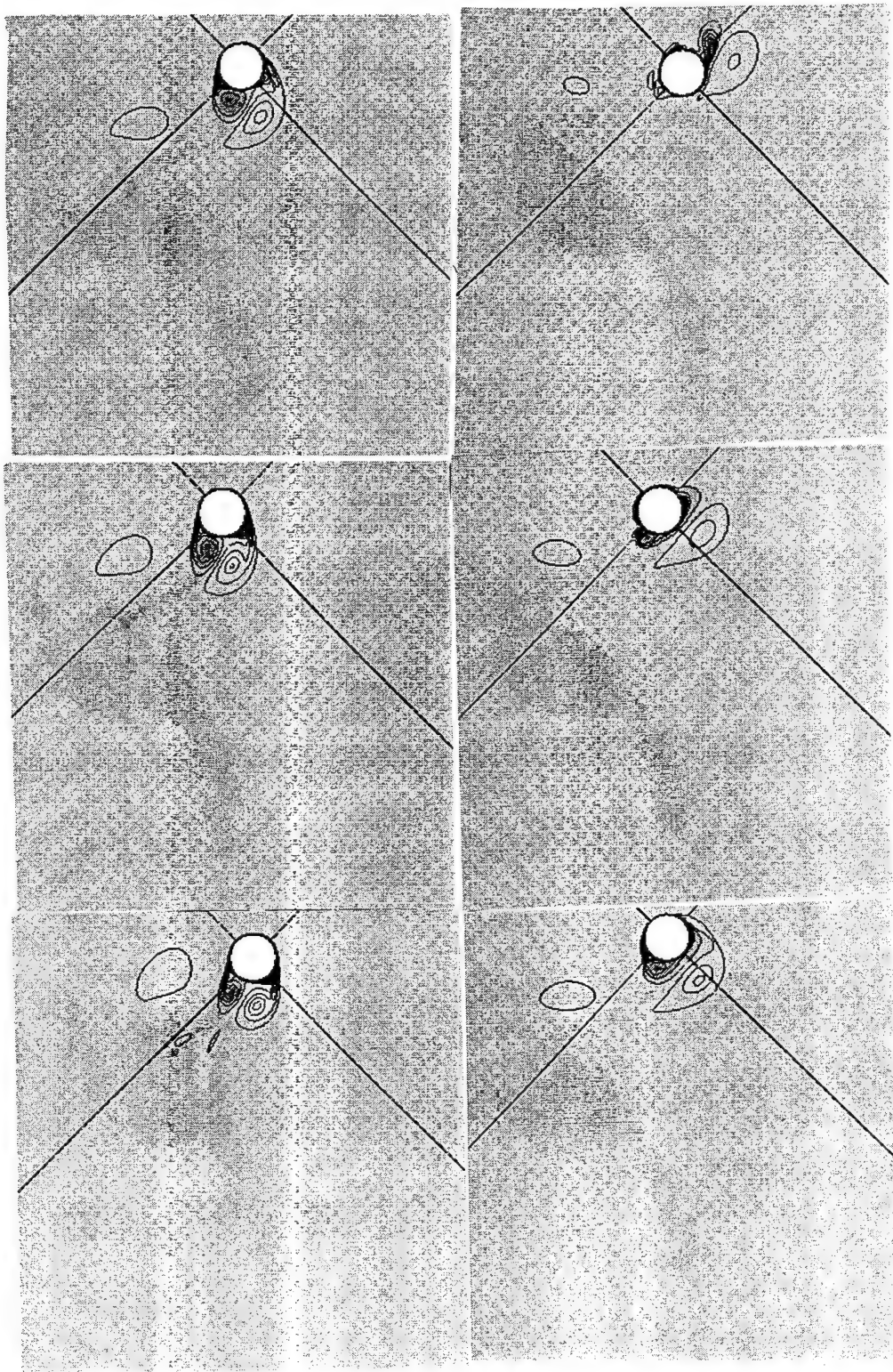


Figure 37. Vorticity Plot for an Oscillatory Flow About a Circular Cylinder at $\beta = 1000$, $K = 12$, $Re = 12,000$
(Steps 1 - 6 in Increments of 22.5 Degrees, Left to Right, Top to Bottom)

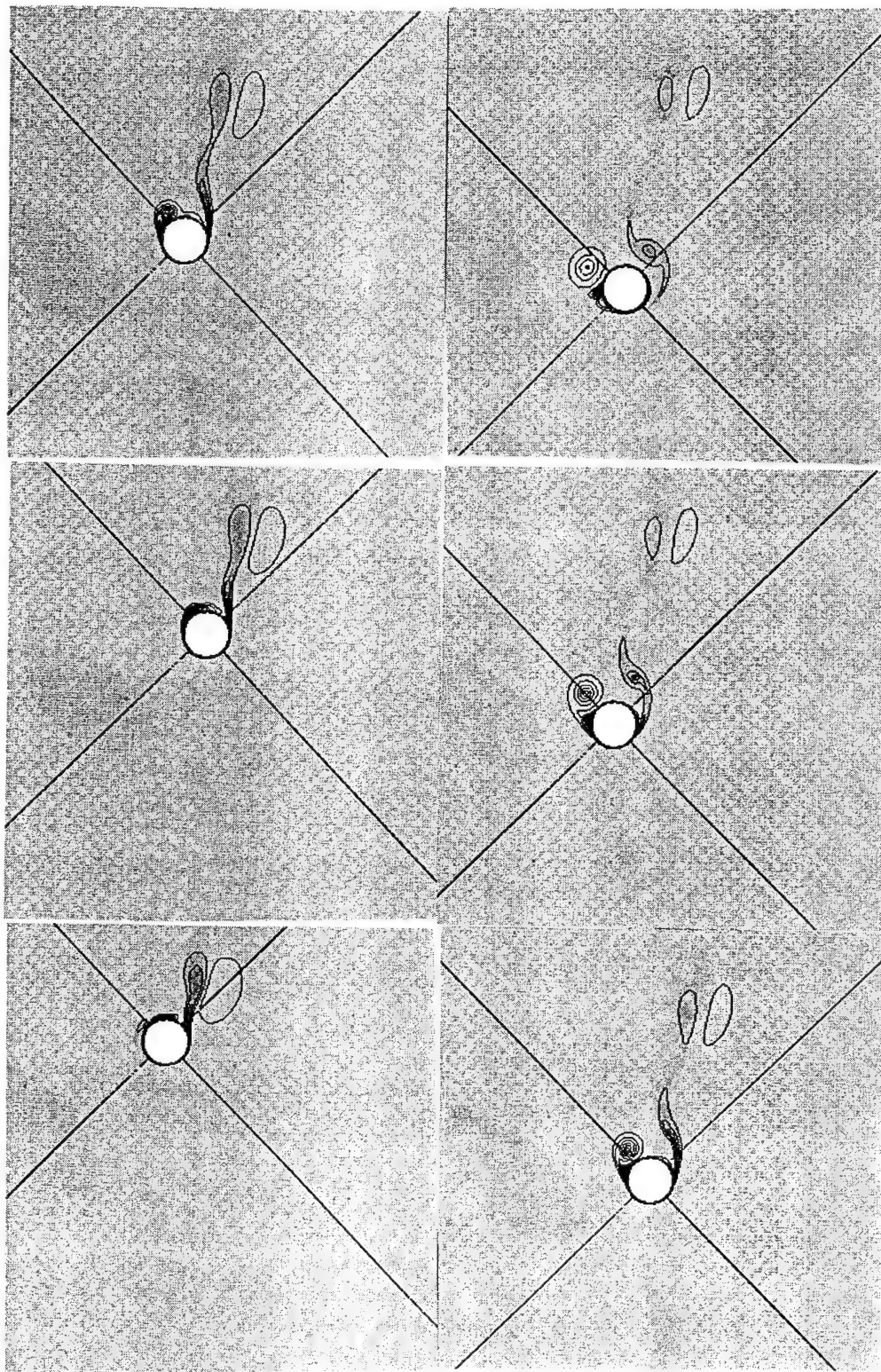


Figure 38. Vorticity Plot for an Oscillatory Flow About a Circular Cylinder at $\beta = 1000$, $K = 12$, $Re = 12,000$
(Steps 7 - 12 in Increments of 22.5 Degrees, Left to Right, Top to Bottom)

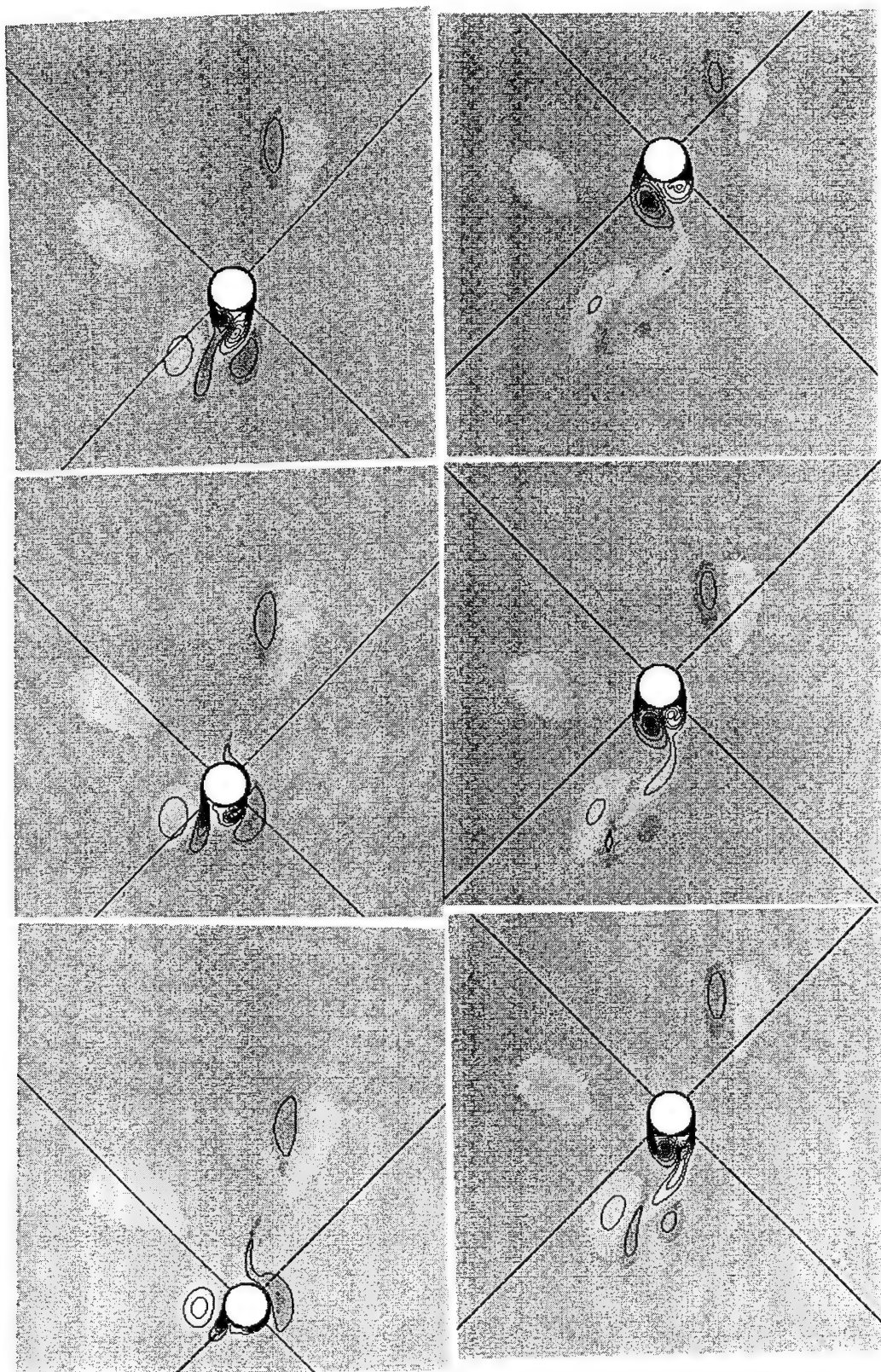


Figure 39. Vorticity Plot for an Oscillatory Flow About a Circular Cylinder at $\beta = 1000$, $K = 12$, $Re = 12,000$
 (Steps 13 - 18 in Increments of 22.5 Degrees, Left to Right, Top to Bottom)

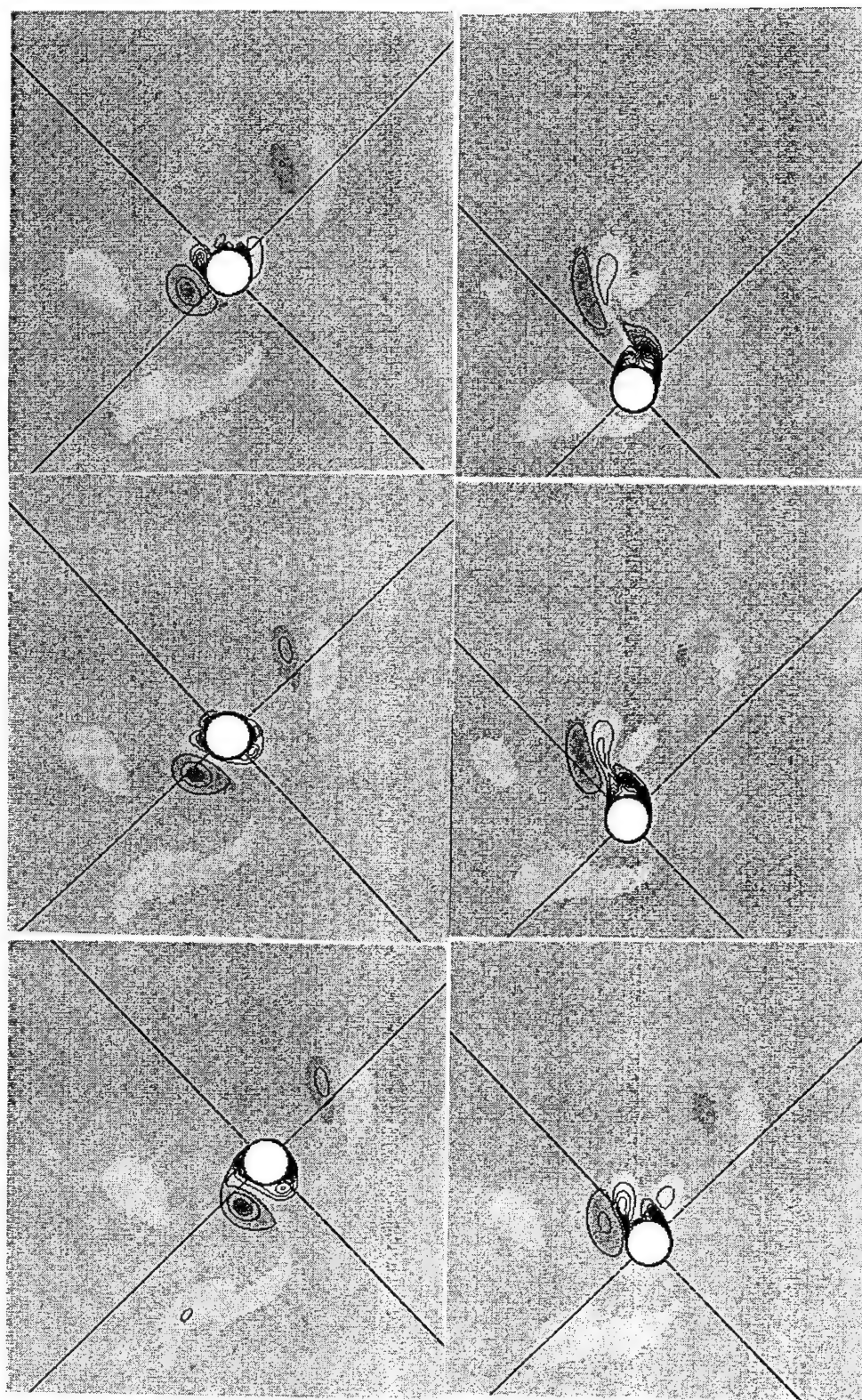


Figure 40. Vorticity Plot for an Oscillatory Flow About a Circular Cylinder at $\beta = 1000$, $K = 12$, $Re = 12,000$
 (Steps 19 - 24 in Increments of 22.5 Degrees, Left to Right, Top to Bottom)

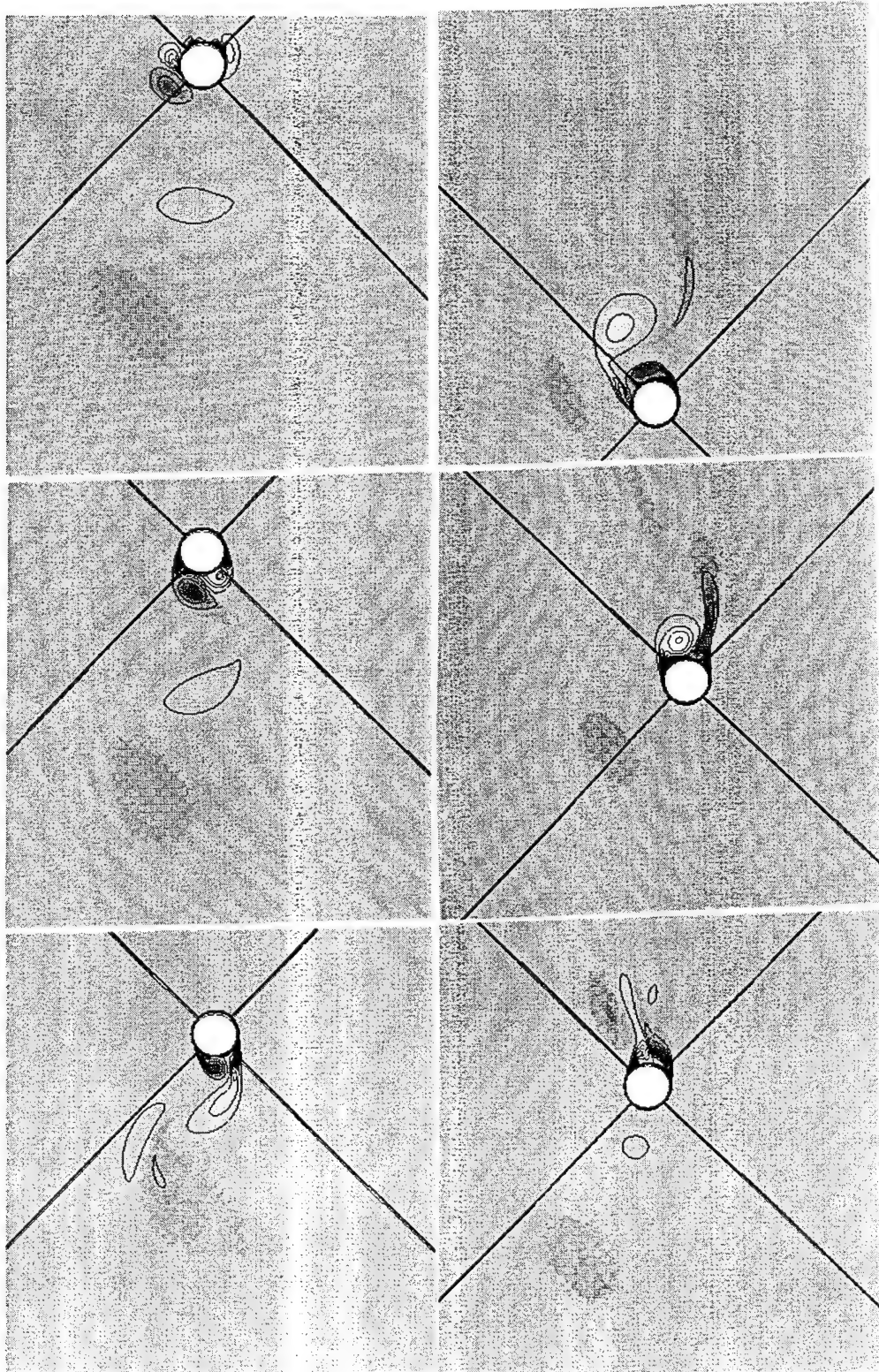


Figure 41. Vorticity Plot for an Oscillatory Flow About a Circular Cylinder at $\beta = 1000$, $K = 20$, $Re = 20,000$
 (Steps 1 - 6 in Increments of 45 Degrees, Left to Right, Top to Bottom)

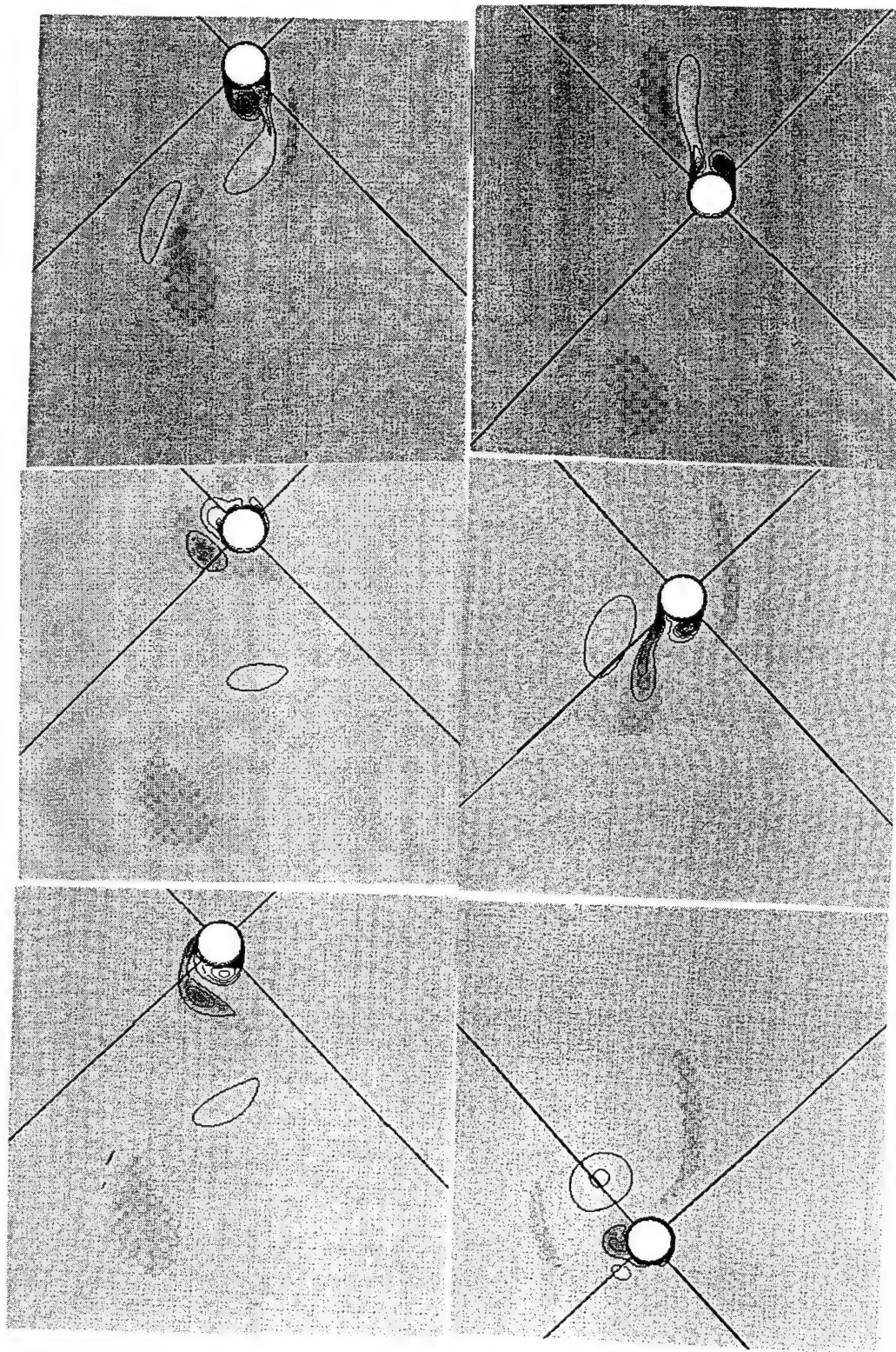


Figure 42. Vorticity Plot for an Oscillatory Flow About a Circular Cylinder at $\beta = 1000$, $K = 20$, $Re = 20,000$
 (Steps 7 - 12 in Increments of 45 Degrees, Left to Right, Top to Bottom)

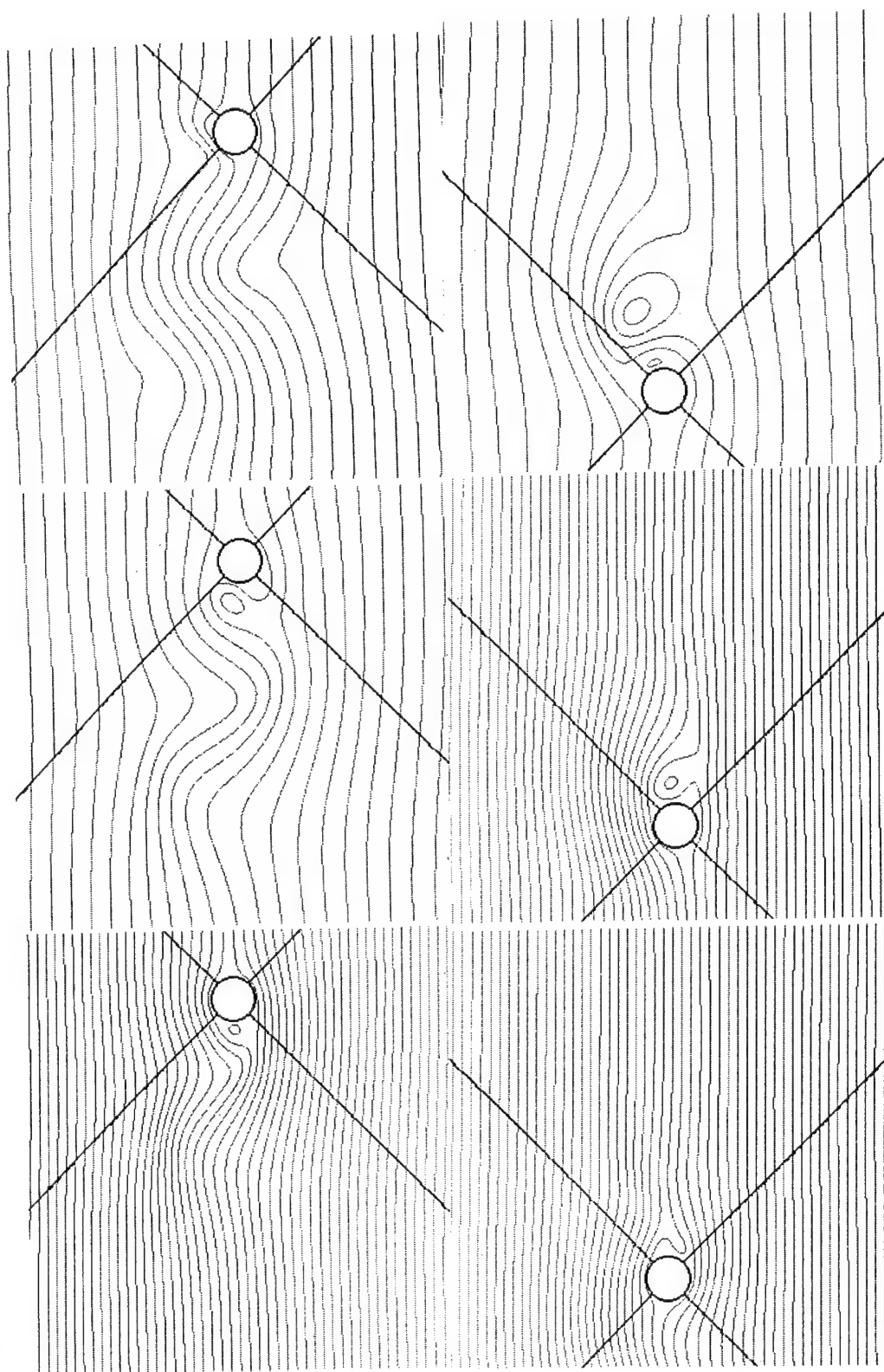


Figure 43. Streamline Plot for an Oscillatory Flow About a Circular Cylinder at $\beta = 1000$, $K = 20$, $Re = 20,000$
(Steps 1 - 6 in Increments of 45 Degrees, Left to Right, Top to Bottom)

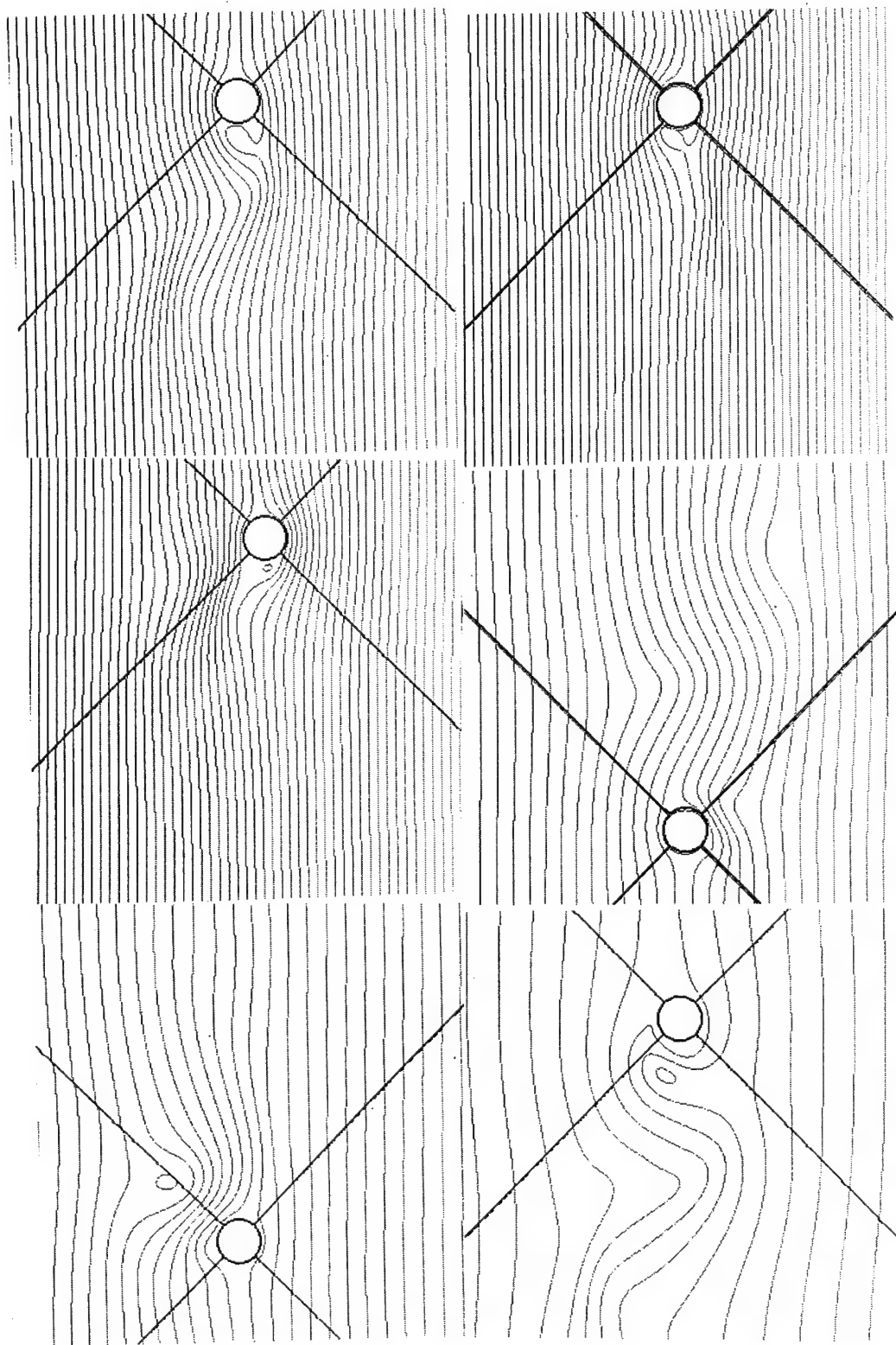


Figure 44. Streamline Plot for an Oscillatory Flow About a Circular Cylinder at $\beta = 1000$, $K = 20$, $Re = 20,000$
(Steps 7 - 12 in Increments of 45 Degrees, Left to Right, Top to Bottom)

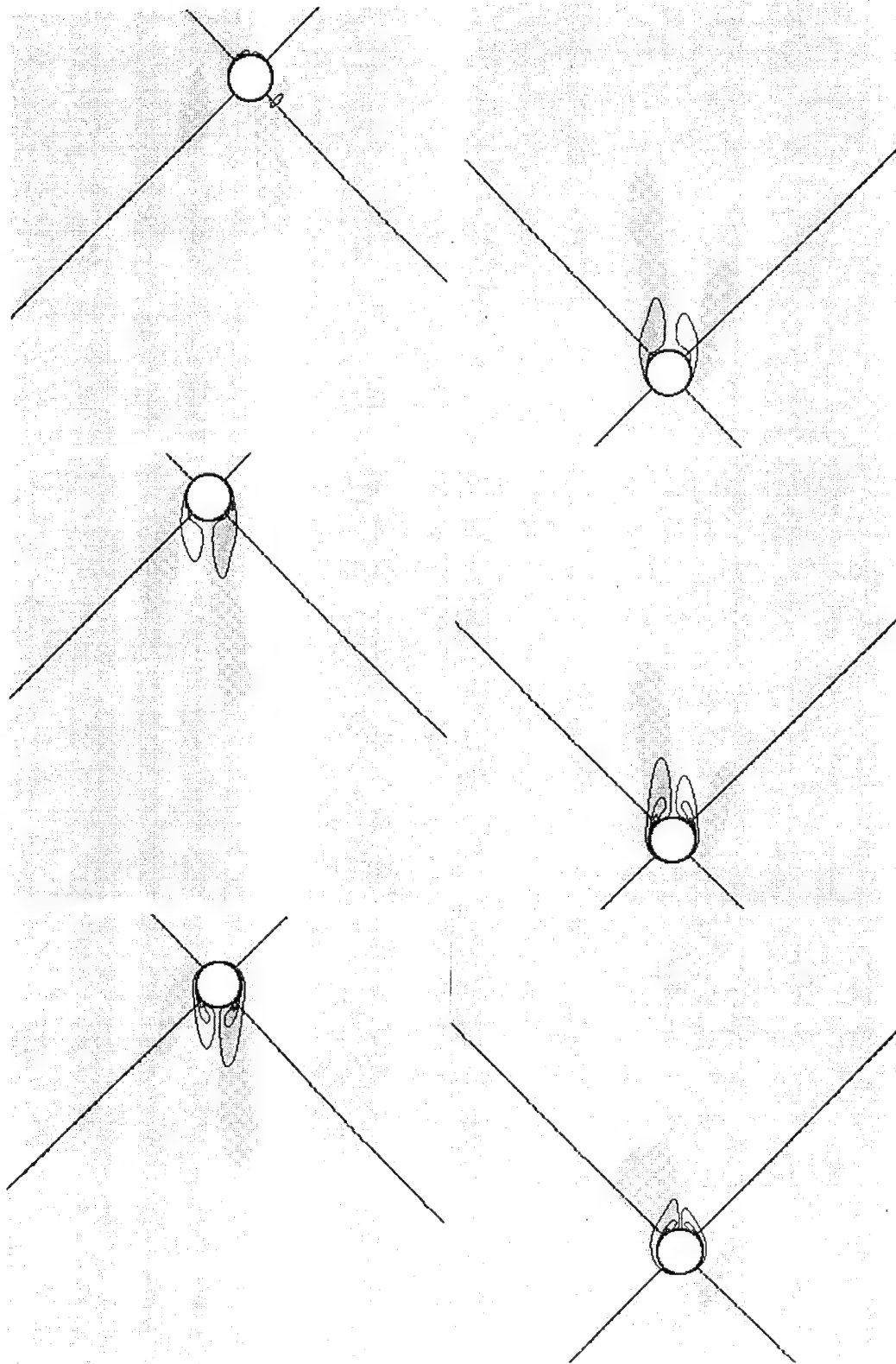


Figure 45. Vorticity Plot for an Oscillatory Flow About a Circular Cylinder at $\beta = 2000$, $K = 20$, $Re = 40,000$
(Steps 1 - 6 in Increments of 45 Degrees, Left to Right, Top to Bottom)

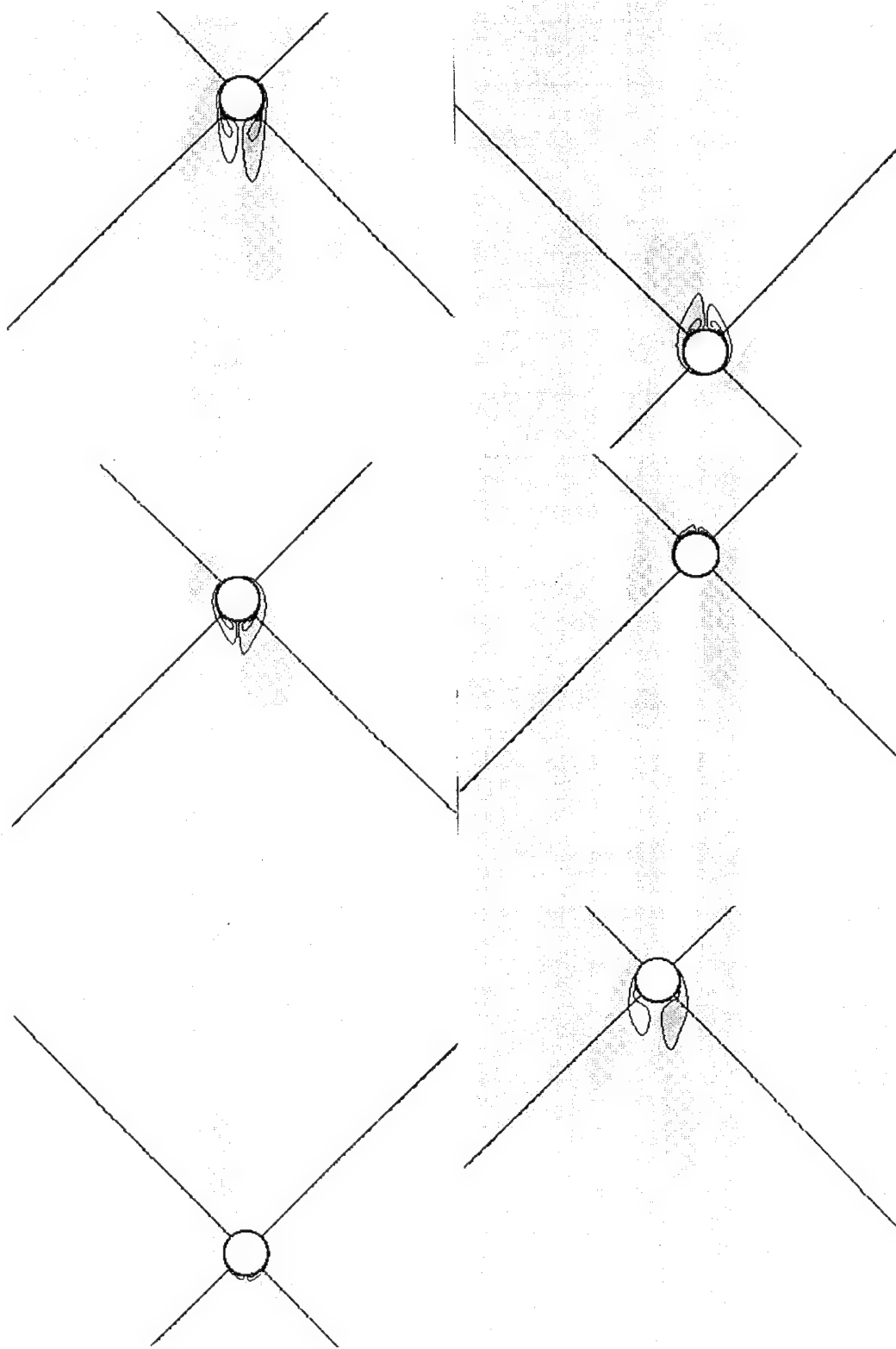


Figure 46. Vorticity Plot for an Oscillatory Flow About a Circular Cylinder at $\beta = 2000$, $K = 20$, $Re = 40,000$
(Steps 7 - 12 in Increments of 45 Degrees, Left to Right, Top to Bottom)

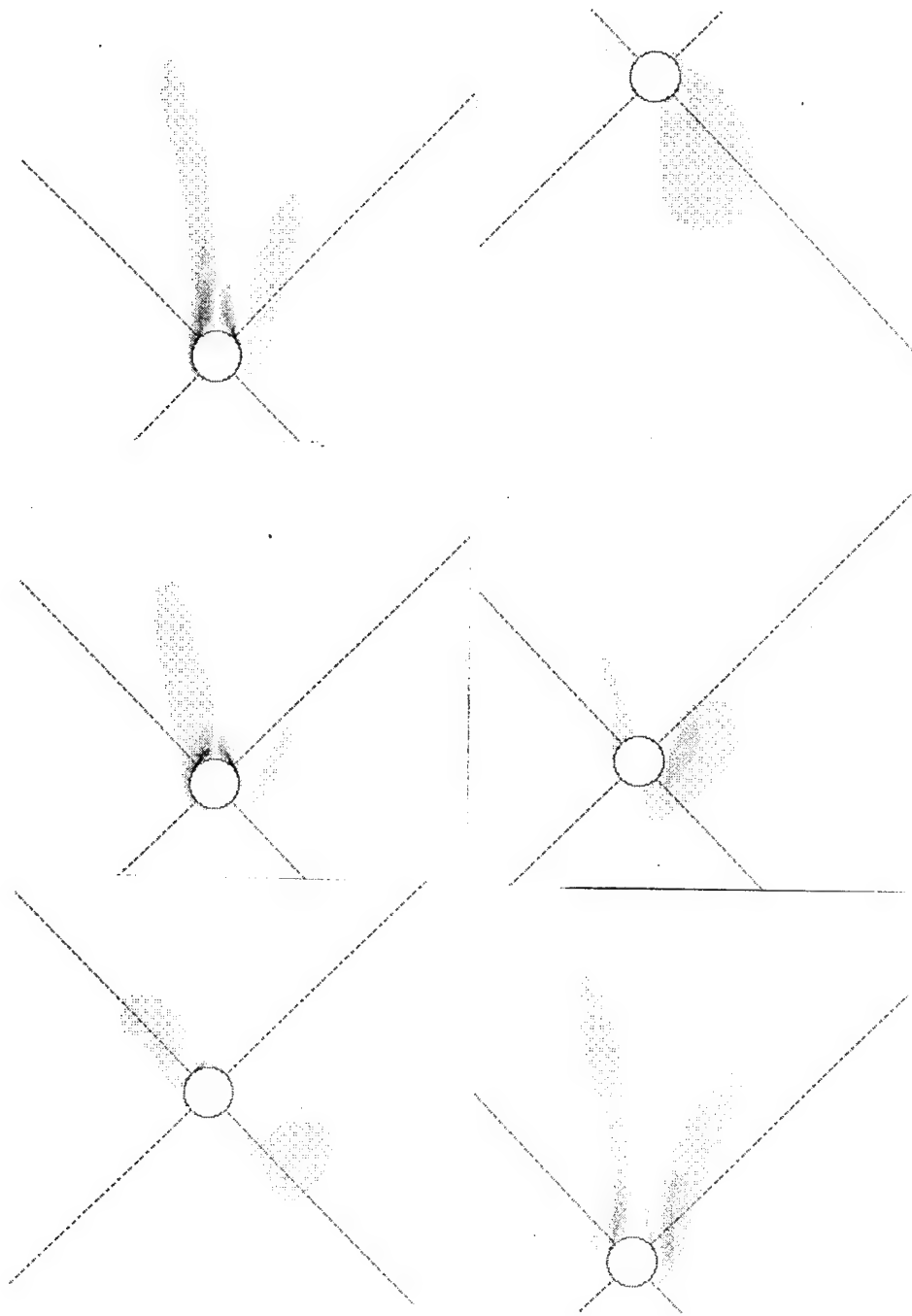


Figure 47. Vorticity Plot for an Oscillatory Flow About a Circular Cylinder at $\beta = 3100$, $K = 35$, $Re = 108,500$
(Steps 1 - 6 in Increments of 45 Degrees, Left to Right, Top to Bottom)

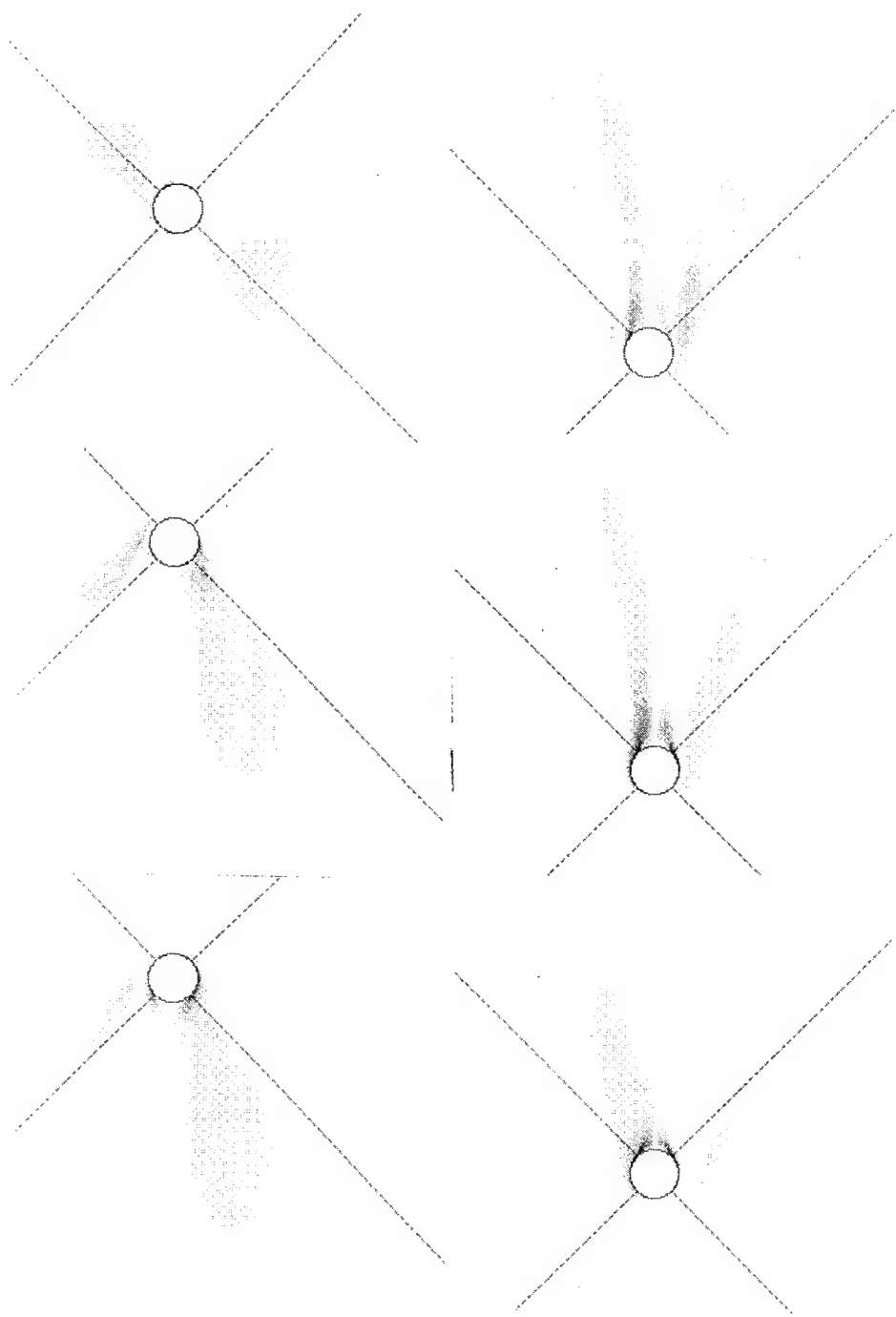


Figure 48. Vorticity Plot for an Oscillatory Flow About a Circular Cylinder at $\beta = 3100$, $K = 35$, $Re = 108,500$
 (Steps 7 - 12 in Increments of 45 Degrees, Left to Right, Top to Bottom)

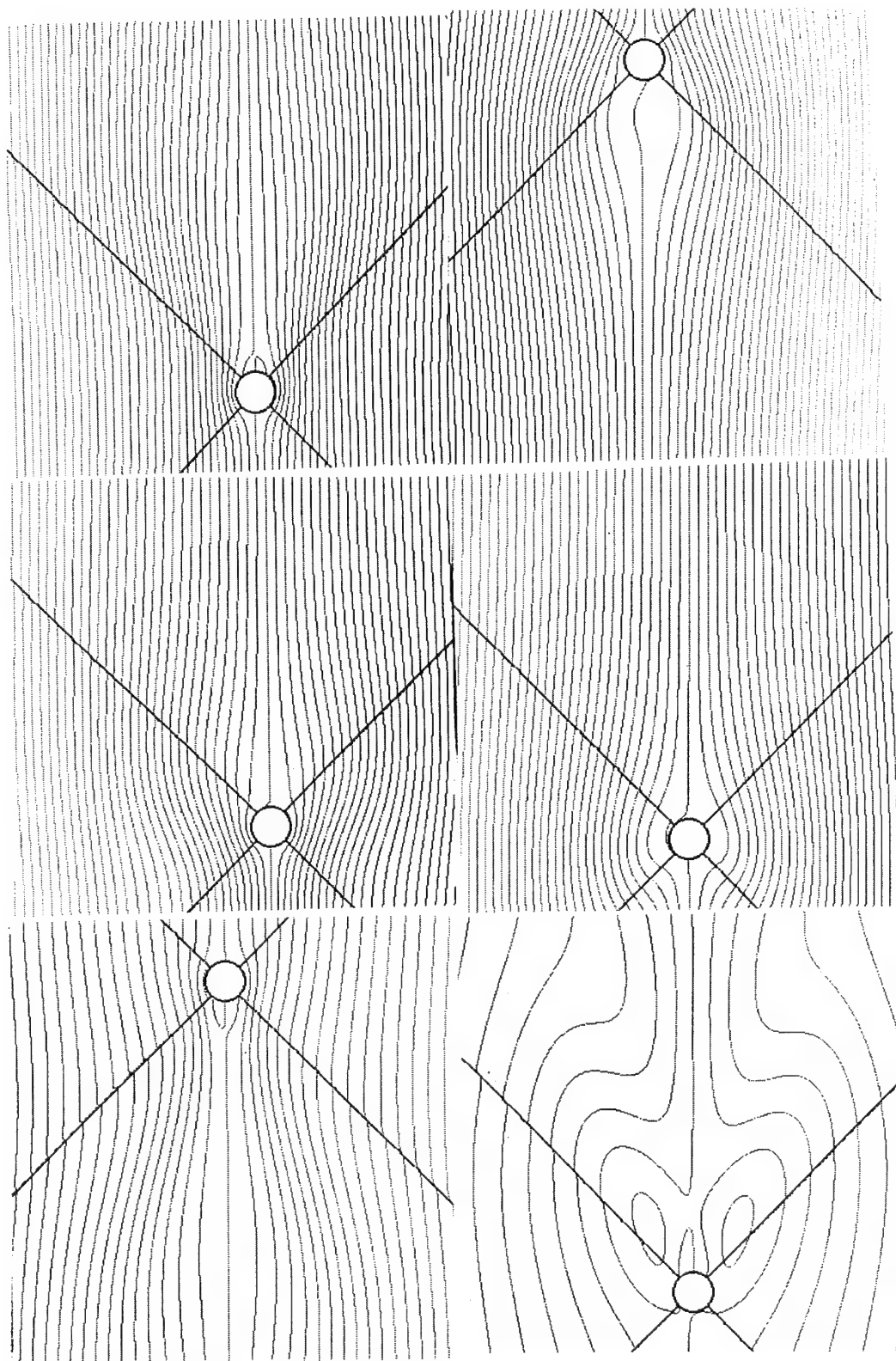


Figure 49. Streamline Plot for an Oscillatory Flow About a Circular Cylinder at $\beta = 3100$, $K = 35$, $Re = 108,500$
(Steps 1 - 6 in Increments of 45 Degrees, Left to Right, Top to Bottom)

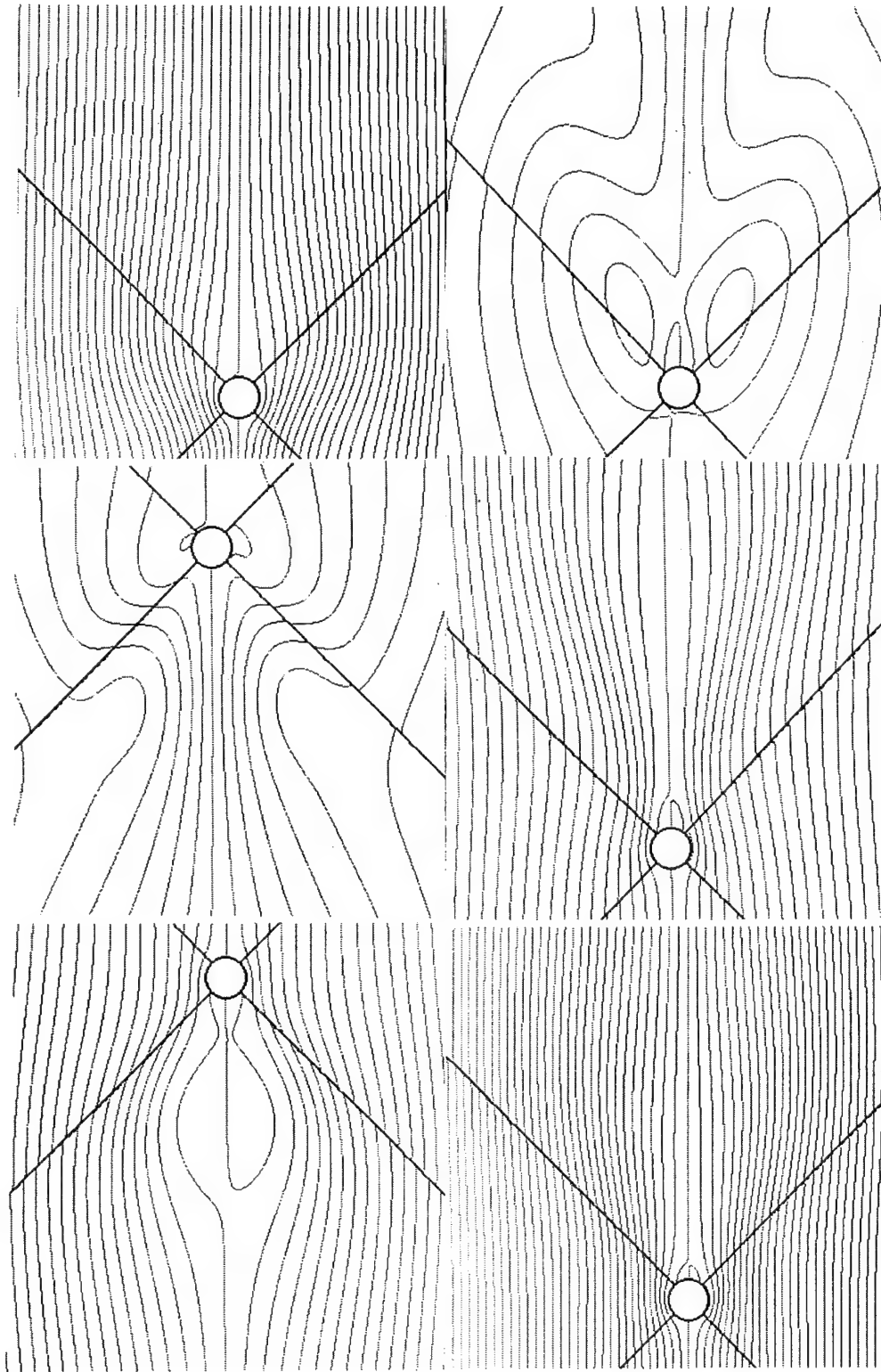


Figure 50. Streamline Plot for an Oscillatory Flow About a Circular Cylinder at $\beta = 3100$, $K = 35$, $Re = 108,500$
 (Steps 7 - 12 in Increments of 45 Degrees, Left to Right, Top to Bottom)

REFERENCES

- Avva, R., Singhal, A., and Lai, Y., 1994, "Numerical Simulation of Periodic and 3-Dimensional Turbulent Flows with CFD-ACE," *ASME Fluids Engineering Division Summer Meeting*, Lake Tahoe, Nevada
- Baba, N., and Miyata, H., 1987, "Higher-Order Accurate Difference Solutions of Vortex Generation from a Circular Cylinder in an Oscillatory Flow," *Journal of Computational Physics*, Vol. 69, pp. 362-369
- Cebeci, T., and Smith, A. M., 1974, *Analysis of Turbulent Boundary Layers*, Academic Press, New York, pp. 47-61
- Comini, G., and Del Giudice, S., 1987, Pressure-Velocity Coupling in Incompressible Fluid Flow," *Annual Review of Numerical Fluid Mechanics and Heat Transfer*, Vol. 1, pp. 33-46
- CFD-ACE Theory Manual, 1993, CFD Research Corporation Huntsville, AL. 35805
- Davis, R. W., and Moore, E. F., 1982, "A Numerical Study of Vortex Shedding from Rectangles," *Journal Fluid Mechanics*, Vol. 116, pp.475-506
- Habachi, S., and Hufford, G., 1995, "Transient Simulation of Turbulent Flow Over Blunt Bodies," CFD Research corporation Huntsville, AL. 35805
- Kato, M., and Launder, B. E., 1993, "The Modelling of Turbulent Flow around Stationary and Vibrating Square Cylinders," *9th Symposium on Turbulent Shear Flows*, Kyoto, Japan
- Keulegan, G., and Carpenter, L., 1958, "Forces on Cylinders and Plates in an Oscillating Fluid," *Journal of Research of the National Bureau of Standards*, Vol. 60, No. 5, pp. 423-440
- Mostafa, S., 1987, "Numerical Simulation of Unsteady Separated Flows," Ph. D. Thesis, Naval Postgraduate School, Monterey, CA
- Murashige, S., Hinatsu, M., and Kinoshita, T., 1989, "Direct Calculations of the Navier-Stokes Equations for Forces Acting on a Cylinder in Oscillatory Flow," *Proceedings of the Eighth International Conference on Offshore Mechanics and Arctic Engineering*, The Hague, The Netherlands, Vol. 2, pp. 411-418
- Putzig, C. J., 1991, "Numerical Experiments in Unsteady Flows through the use of Full Navier-Stokes Equations," M.S. Thesis, Naval Postgraduate School, Monterey, CA
- Rogers, S., 1994, "Progress in High-Lift Aerodynamic Calculations," *Journal of Aircraft*, Vol. 31, No. 6, pp. 1244-1251

Sarpkaya, T., 1976, "Vortex Shedding and Resistance in Harmonic Flow About Smooth and Rough Circular Cylinders at High Reynolds Numbers," Naval Postgraduate School Technical Report No. 59SL76021

Sarpkaya, T., Putzig, C., Gordon, D., Wang, X., and Dalton, C., 1992, "Vortex Trajectories Around a Circular Cylinder in Oscillatory Plus Mean Flow," *Journal of Offshore Mechanics and Arctic Engineering*, Vol. 114 pp.291-298

Storm, M., 1984, "Wave and Current Induced Forces on Cylinders," M.S. Thesis, Naval Postgraduate School, Monterey, CA

INITIAL DISTRIBUTION LIST

	No. Copies
1. Defense Technical Information Center 8725 John J. Kingman Rd., STE 0944 Ft. Belvoir, Virginia 22060-6218	2
2. Library, Code 52 Naval Postgraduate School Monterey, California 93943-5101	2
3. Department Chairman, Code ME Department of Mechanical Engineering Naval Postgraduate School Monterey, CA 93942-5000	2
4. Professor T. Sarpkaya, Code ME-SL Department of Mechanical Engineering Naval Postgraduate School Monterey, CA 93942-5000	5
5. Curricular Officer, Code 34 Department of Mechanical Engineering Naval Postgraduate School Monterey, CA 93942-5000	1
6. LCDR Craig D. Hanson 529 Fenwick Dr. San Antonio, TX 78239	2